Molecular Biology of the Cell
Vol. 19, 572–586, February 2008

Sequestration of Mutated α1-Antitrypsin into Inclusion Bodies Is a Cell-protective Mechanism to Maintain Endoplasmic Reticulum Function

Susana Granell,* Giovanna Baldini,† Sameer Mohammad,* Vanessa Nicolin,† Paola Narducci,† Brian Storrie,‡ and Giulia Baldini*

*Department of Biochemistry and Molecular Biology and ‡Department of Physiology and Biophysics, University of Arkansas for Medical Sciences, Little Rock, AR 72205; and †Dipartimento Universitario Clinico di Biomedicina, Universita' degli Studi di Trieste, Trieste I-34138, Italy

Submitted June 21, 2007; Revised October 18, 2007; Accepted November 16, 2007
Monitoring Editor: Thomas Sommer

A variant α1-antitrypsin with E342K mutation has a high tendency to form intracellular polymers, and it is associated with liver disease. In the hepatocytes of individuals carrying the mutation, α1-antitrypsin localizes both to the endoplasmic reticulum (ER) and to membrane-surrounded inclusion bodies (IBs). It is unclear whether the IBs contribute to cell toxicity or whether they are protective to the cell. We found that in hepatoma cells, mutated α1-antitrypsin exited the ER and accumulated in IBs that were negative for autophagosomal and lysosomal markers, and contained several ER components, but not calnexin. Mutated α1-antitrypsin induced IBs also in neuroendocrine cells, showing that formation of these organelles is not cell type specific. In the presence of IBs, ER function was largely maintained. Increased levels of calnexin, but not of protein disulfide isomerase, inhibited formation of IBs and lead to retention of mutated α1-antitrypsin in the ER. In hepatoma cells, shift of mutated α1-antitrypsin localization to the ER by calnexin overexpression lead to cell shrinkage, ER stress, and impairment of the secretory pathway at the ER level. We conclude that segregation of mutated α1-antitrypsin from the ER to the IBs is a protective cell response to maintain a functional secretory pathway.

INTRODUCTION

The serpin family of protease inhibitors and in particular two of its members, α1-antitrypsin (AAT) and neuroserpin, provide well-studied examples of how small changes in protein conformation lead to cell toxicity (Kopito and Ron, 2000; Perlmutter, 2002b; Carrell, 2005; Lomas, 2005). A variant α1-antitrypsin with E342K mutation (ATZ) has greatly increased tendency to form homodimers and higher order polymers compared with AAT (Huntington *et al*., 1999; Lomas *et al*., 2005). PiZZ individuals (homozygotes for ATZ; Perlmutter, 2002b) have reduced release of the serpin in the blood, which leads to an unbalanced activity of neutrophil proteases in the lung and damage to the alveolar tissue. Some PiZZ individuals have also liver disease due to intracellular retention of the mutated protein (Perlmutter, 2002a). Early ultrastructural studies of hepatic biopsies from children with the PiZZ mutation show accumulation of ATZ in dilated sections of the ER, indicating that the misfolded protein accumulates in this compartment (Feldmann *et al*., 1974; Yunis *et al*., 1976; Hultcrantz and Mengarelli, 1984). More recently, it has been found that ATZ also accumulates in membrane-surrounded inclusion bodies (IBs) that have the morphological appearance of autophagosomes (Teckman and Perlmutter, 2000). However, in livers from transgenic mice that express both ATZ and the autophagosome marker LC3-green fluorescent protein (GFP), the marker did not colocalize with the ATZ containing IBs (Kamimoto *et al*., 2006). In contrast, in cells where autophagic activity was inhibited, there was increased number of ATZ-containing IBs (Kamimoto *et al*., 2006). Therefore, although it seems that the autophagic response is important for ATZ disposal, it is not known to which extent ATZ-containing IBs correspond to autophagosomes. In addition to ATZ, aggregation of other proteins in the secretory pathway leads to formation of membrane-surrounded IBs that are separate from the ER, from pre-Golgi intermediates, or both. Examples are the Russell bodies formed in response to expression of mutated immunoglobulins in myeloma cells, IBs in response to accumulation of misfolded proinsulin in the β-cells of the Akita mouse, and myelin-like figures in Schwann cells in response to expression of mutated peripheral myelin protein-22 (Dickson *et al*., 2002; Zuber *et al*., 2004; Mattioli *et al*., 2006). It is not clear whether formation of the IBs is a cause of cell toxicity or a cell-protective mechanism. This issue is currently being investigated with respect to the IBs that originate in the cytoplasm from sequestration of aggregated proteins, such as aggresomes containing ΔF508 mutant form of cystic fibrosis transmembrane conductance regulator and huntingtin filaments. The aggresomes are different from the ATZ-containing IBs or the Russell bodies because they are not membrane-surrounded (Kopito and Sitia, 2000). With

This article was published online ahead of print in *MBC in Press* (http://www.molbiolcell.org/cgi/doi/10.1091/mbc.E07–06–0587) on November 28, 2007.

Address correspondence to: Giulia Baldini (gbaldini@uams.edu).

Abbreviations used: AAT, wild-type α1-antitrypsin; ATZ, mutated α1-antitrypsin E342K; ER, endoplasmic reticulum; GFP, green fluorescent protein; IB, inclusion body; N2A, mouse neuroblastoma Neuro2A; NHK, α1-antitrypsin null Hong Kong; PDI, protein-disulfide isomerase; ROI, region of interest; TIRFM, total internal reflection microscopy; UPR, unfolded protein response.

respect to the aggresomes, it seems that cell toxicity actually precedes the formation of IBs (Bennett *et al*., 2005; Diaz-Hernandez *et al*., 2006) and that their formation reduces neuronal death (Arrasate *et al*., 2004). However, the question as to whether membrane-surrounded IBs, such as those containing ATZ, are themselves toxic or, rather, protective to the cell has not yet being addressed.

In the ER, ATZ interacts with a variety of ER chaperones, including calnexin, protein-disulfide isomerase (PDI), GRP-78/BiP, and with the *N*-glycan modifying enzymes UDP-glucose:glycoprotein glucosyltransferase and α-mannosidase-like protein (Cabral *et al*., 2002; Oda *et al*., 2003; Schmidt and Perlmutter, 2005; Papp *et al*., 2006). Binding and release of ATZ from calnexin are necessary for ATZ degradation (Cabral *et al*., 2002; Oda *et al*., 2003; Sifers, 2004). Misfolded proteins are then retrotranslocated from the ER lumen to the cytosol and degraded by the ubiquitin-proteasome system known as ER-associated degradation (ERAD) (Meusser *et al*., 2005; Ruddock and Molinari, 2006). Here, we have defined the IBs as sites of ATZ localization segregated from the main ER. Whether calnexin or other chaperones function to control ATZ transit to the IBs and whether formation of ATZ-containing IBs is protective to the cell are major questions addressed in this article.

MATERIALS AND METHODS

Reagents and Antibodies

Lipofectamine 2000, primers, and Alexa Fluor^{546}-Phalloidin were purchased from Invitrogen (Carlsbad, CA). Mouse monoclonal antibody against hemagglutinin (HA) (12 CA5), peroxidase (POD)-conjugated anti-HA antibody, secondary peroxidase-conjugated anti-mouse immunoglobulin (Ig)G, protease inhibitor cocktail (Complete Mini), and pepstatin were from Roche Applied Science (Indianapolis, IN). The rabbit polyclonal antibodies against calnexin and GRP-78/BiP, and mouse monoclonal anti-PDI and anti-KDEL were from Stressgen (San Diego, CA). The mouse monoclonal anti-Myc and anti-insulin antibodies and the rabbit polyclonal anti-Myc and anti-insulin antibodies were from Santa Cruz Biotechnology (Santa Cruz, CA). Mouse monoclonal antibodies against AAT and actin were from Chemicon International (Temecula, CA). The rabbit polyclonal antibodies against GM130 were from BD Bioscience (San Jose, CA). The rabbit polyclonal against neuroserpin was purchased from Abcam (Cambridge MA). Cyanine (Cy)3, fluorescein isothiocyanate (FITC), and Cy5-conjugated anti-mouse and anti-rabbit IgG were from Jackson ImmunoResearch Laboratories (West Grove, PA). Enhanced chemiluminescence detection kits were purchased from PerkinElmer Life and Analytical Sciences (Boston, MA). Nocodazole, 1,4-diazabicyclo[2.2.2]octane, 3-methyladenine, tunicamycin, and phenylmethanesulfonyl fluoride (PMSF) were from Sigma-Aldrich (St. Louis, MO). Protein G-Sepharose Fast Flow was from GE Healthcare (Little Chalfont, Buckinghamshire, United Kingdom).

Cell Culture and Transfection

Mouse hepatoma Hepa 1-6, human hepatoma Huh-7, and mouse neuroblastoma Neuro2A (N2A) cell lines were cultured in DMEM with 10% bovine serum and 5% penicillin/streptomycin. Cells were transiently transfected with the indicated plasmids by using Lipofectamine 2000 according to the manufacturer's instructions.

cDNAs and Constructs

The enhanced green fluorescent protein (EGFP) expression vector pEGFP-N2 was purchased from Clontech (Mountain View, CA). The cDNA for human AAT, neuroserpin, and proinsulin were obtained from Origene Technologies (Rockville, MD). PDI-pCMV-SPORT6 was purchased from the American Type Culture Collection (Manassas, VA). Construction of the plasmids Myc-AAT-pcDNA3.1, HA-ATZ-pcDNA3.1, Myc-ATZ-pcDNA3.1, ATZ-GFP, neuroserpin Portland-pcDNA3.1, proinsulin-pcDNA3.1, calnexin-pcDNA3.1, and calnexin-GFP are described in Supplemental Material. Lysosomal-associated membrane protein 1 (LAMP1)-GFP was a kind gift from Dr. J. Lippincott-Schwartz and LC3-GFP was a kind gift from Dr. T. Yoshimori.

Immunoprecipitations

Transfected cells grown in 100-mm dishes were scraped in immunoprecipitation (IP) buffer (100 mM Tris-HCl, pH 7.4, 50 mM NaCl, 1% NP-40, and protease inhibitors [Complete Mini, 1 μM pepstatin, and 1 mM PMSF]) and incubated for 30 min at 4°C. Cell lysates were rotated for 1 h at 4°C with the indicated antibody. After addition of protein G beads, the samples were further incubated for 1 h at 4°C. After four washes with IP buffer and one wash with a high salt buffer (150 mM Tris, pH 7.4, 400 mM NaCl, and 1% NP-40 at pH 8.0), the beads were resuspended in sample buffer, boiled for 5 min, and centrifuged. Supernatants and cell extracts were loaded onto a 7% SDS-polyacrylamide gel electrophoresis (PAGE) gel.

Preparation of Cell Lysates

To measure the amount of cell ATZ, transiently transfected Hepa 1-6 cells were grown in 30-mm dishes, and, at the indicated times, cells were washed once in Kglu buffer (20 mM HEPES, pH 7.4, 120 mM potassium glutamate, 20 mM potassium acetate, 5 mM EGTA, and 1 mg/ml bovine serum albumin) and scraped from plates in Kglu buffer containing 1% Triton X-100 and proteases inhibitors (Complete Mini, 1 μM pepstatin, and 1 mM PMSF). Samples were passed five times through a 27-gauge$^{1/2}$ needle and incubated 30 min at 4°C. Cell lysates were centrifuged at 7200 × *g* for 10 min, and the pellet was discarded. Cell lysates were electrophoresed on a 7% SDS-PAGE gel by using loading buffer with or without SDS and β-mercaptoethanol (denaturing and nondenaturing conditions, respectively).

Immunoblotting

Separated proteins were transferred to a nitrocellulose membrane probed with the indicated primary antibodies and secondary POD-conjugated antibodies. Enhanced chemiluminescence detention, densitometry, and protein determination were performed as described previously (Wang *et al*., 1997).

Sucrose Gradient Centrifugation

Transiently transfected Hepa 1-6 were grown in 100-mm dishes, washed once in Kglu buffer, and scraped from plates in Kglu buffer containing proteases inhibitors. Samples were passed 10 times through a 27-gauge$^{1/2}$ needle. Postnuclear supernatant (PNS) was obtained by centrifugation at 100 × *g* for 5 min. The pellet obtained by further centrifugation of the PNS at 1000 × *g* for 10 min was resuspended in Kglu buffer containing protease inhibitors and loaded on the top of a sucrose density gradient (30–50%, wt/vol). The gradient was centrifuged for 2 h at 45,000 rpm in a Beckman Optima TLX ultracentrifuge (TLS-55 swinging rotor), and 19 fractions were collected. The fractions obtained were electrophoresed on a 7% SDS-PAGE gel by using loading buffer with SDS and β-mercaptoethanol.

Cell Sorting and Electron Microscopy

Hepa 1-6 cells plated in 100-mm dishes were transiently transfected with ATZ-GFP or pcDNA3.1 (mock-transfected cells). Forty-eight hours after transfection, cells were trypsinized and centrifuged at 300 × *g* for 3 min. The pellet was resuspended in a filter-sterilized sorting buffer (phosphate-buffered saline [PBS], 25 mM HEPES, pH 7.0, 2% fetal bovine serum [FBS], and 1 mM EDTA). Cells transiently expressing ATZ-GFP were sorted by flow cytometry using a FACSAria instrument (BC Biosciences, San Jose, CA). The brightest population of GFP-positive cells (top 30%) was recovered for the electron microscopy in 10 ml of complete growth medium and centrifuged for 10 min at 1500 × *g*. The pellets were rinsed with PBS and fixed with 2% glutaraldehyde in phosphate buffer, pH 7.4, for 1 h at room temperature. Cells were rinsed twice with PBS containing 0.01% sodium azide and processed for electron microscopy as described previously (Baldini *et al*., 1998).

Control cells were kept in complete medium (DMEM, 10% FBS, and 5% penicillin/streptomycin) during the sorting process (45 min).

Fluorescence Microscopy

Immunofluorescence staining was performed as described previously (Mohammad *et al*., 2007). Epifluorescence and confocal fluorescence images were captured with a CARV I spinning confocal imaging system (BioVision Technologies, Exton, PA) attached to an X-71 fluorescence microscope (Olympus, Tokyo, Japan). Images were collected using a CoolSNAP HQ camera (Photometrics, Tucson, AZ), and processed by using the IPLab software (Scanalytics, Fairfax, VA). For some experiments, ATZ-GFP distribution in Hepa 1-6 cells was visualized by total internal reflection microscopy (TIRFM) by using an X-71 inverted microscope equipped with an argon laser (488 nm). For these experiments, cells in DMEM were visualized 48 h after transfection. Images were collected using a CoolSNAP HQ camera and processed using MetaMorph software (Molecular Devices, Sunnyvale, CA).

Autophagy Assays

Before analysis, Hepa 1-6 cells were starved for 6 h in Hanks' balanced salt solution (HBSS) (HBSS, starvation medium) or maintained in normal growth media (Pattingre *et al*., 2005). Autophagy was inhibited by preincubation of the cells with 10 mM 3-methyladenine for 30 min before amino acid deprivation. To quantify the level of autophagy, the number of GFP-LC3 dots per cell was determined by manual counting.

Colocalization of ATZ with Calnexin

For the quantification of calnexin expression, fluorescence intensity was measured by manually tracing the outline of individual cells and by measuring the pixel intensity of the selected area by using the IPLab software. Confocal fluorescent images of the cells were analyzed for colocalization of ATZ with calnexin by using IPLab. Briefly, after autosegmentation of calnexin fluorescence (green channel) and Myc-ATZ fluorescence (red channel), the regions of interest were analyzed by measuring the Mander's overlap coefficient M1 (Manders *et al*., 1992). M1 is defined as the ratio of the summed intensities of pixels from the green image for which the intensity of the red is above zero. In our experimental conditions, M1 indicates pixel intensity overlap from channel 1 (green, calnexin) to channel 2 (red, Myc-ATZ).

Quantification of Hepa 1-6 Cell Area

To quantify the area of the cells, epifluorescence images were obtained with constant parameters of acquisition. The region of interest (ROI) was selected by manually drawing the cell margins after the F-actin staining for each individual cell. The intensity of the fluorescence in the different channels and the area of the selected ROIs were measured by using IPLab software. The amount of ATZ in each positive cell was calculated by subtracting the background (pixel intensity of the neighboring nontransfected cells) from the total pixel intensity of ATZ-GFP.

Quantification of the Increase of the Unfolded Protein Response (UPR) by Immunofluorescence

Epifluorescence images were obtained with constant parameters of acquisition. The ROI was selected by manually drawing the cell margins following KDEL staining for each individual cell. Fluorescence pixel intensity in the two different channels (blue, calnexin; red, KDEL) was measured by using IPLab software. As a positive control, UPR was induced by incubating the cells with 1 μg/ml tunicamycin for 16 h.

Quantification of Increase of Intracellular ATZ versus Overexpression of Calnexin and PDI

Epifluorescence images were obtained with constant parameters of acquisition. The ROI was selected by manually drawing the cell margins after calnexin or PDI staining. IPLab software was used to calculate the intensity of the fluorescence in the different channels (green, PDI or calnexin; red, Myc-ATZ) of the selected ROI. First, we measured the average pixel intensity of intracellular ATZ in cells expressing Myc-ATZ alone (n = 30). The -fold increase of intracellular ATZ was calculated by the following ratio: pixel intensity of Myc-ATZ (red channel) coexpressed with either exogenous calnexin or PDI/pixel intensity of Myc-ATZ in cells expressing ATZ alone. Calnexin and PDI overexpression was calculated by the following ratio: pixel intensity of calnexin or PDI in cotransfected cells/pixel intensity calnexin or PDI of the neighboring nontransfected cells (n = 3 per transfected cell).

Quantification of Area of ATZ-containing Compartment

After autosegmentation of Myc-ATZ fluorescence (red channel) in confocal images, the area of the regions of interest was measured using IPLab software.

Colocalization of ATZ with Insulin

Confocal fluorescent images were retrieved, and colocalization of ATZ with insulin was measured by using the Mander's overlap coefficient M1 (IPLab software) (Manders *et al*., 1992). For these experiments, the colocalization coefficient M1 indicates pixel intensity overlap from channel 1 (red, Myc-ATZ) to channel 2 (green, insulin).

Quantification of Neurite Outgrowth

To measure neurite outgrowth, cells were serum starved for 24 h. Cell F-actin staining visualized by epifluorescence microscopy was used to classify the cells into two categories: cells with neurites or cells without neurites. We considered neurites the processes that were at least half the length of the cell body. The length of the neurite was analyzed by using IPLab software.

Nocodazole Treatment

Hepa 1-6 cells were transiently transfected with ATZ-GFP, and 48 h after transfection cells, were incubated for 6 h in complete culture medium with 80 μM nocodazole or vehicle (dimethyl sulfoxide) at 37°C. After the incubation period, cells were washed, fixed, and processed for immunofluorescence.

Insulin and Proinsulin Measurements

To measure proinsulin release in the medium, transfected Hepa 1-6 cells grown in 30-mm dishes were washed with M2 medium (20 mM HEPES, pH 7.4, 150 mM NaCl, 5 mM KCl, 1 mM $MgCl_2$, 1 mM $CaCl_2$, and 0.1 mg/ml bovine serum albumin) and incubated at 37°C for the indicated times in 1 ml of the same medium with 5 mM glucose. The medium was collected and centrifuged at 300 $\times$ *g* for 3 min to remove cell debris. To measure proinsulin and insulin in the cell, transiently transfected Hepa 1-6 and N2A cells were grown in 30-mm dishes, and, at the indicated times, cells were washed once in Kglu buffer and scraped from plates in Kglu buffer containing 1% Triton X-100 and proteases inhibitors. Cells were homogenized by passing them five times through a needle (27-gauge$^{1/2}$), and then they were incubated for 30 min at 4°C. Cell extracts were obtained by centrifugation at 7200 $\times$ *g* for 10 min. All the measurements were done 48 h after transfection. Insulin and proinsulin levels in cell extracts and cell-free medium were measured using the human insulin and proinsulin enzyme-linked immunosorbent assay (ELISA) kit from Linco Research (St. Charles, MO) according to the manufacturer's instructions.

Statistical Analysis

All experiments were done at least twice, and data are expressed as mean $\pm$ SD from a single experiment unless noted otherwise. After checking that the measures realized were normally distributed, two-tailed Student's *t* tests were performed.

RESULTS

ATZ Expression in Hepatoma Cells Induces IB Formation in a Time-dependent Manner

To study the cell distribution of ATZ, HA-ATZ was transiently transfected in mouse hepatoma Hepa 1-6 cells (Figure 1A). At 24 h after transfection, ATZ had a reticular pattern in 80.6 $\pm$ 7.92% of the cells and colocalized with calnexin in the ER. At 48 h, cells with ATZ in a reticular pattern decreased to 29.3 $\pm$ 2.12% of the cell population (Figure 1B) and ATZ occurred predominantly as cytoplasmic puncta (IBs; area = 2.25 $\pm$ 1.29 μm^2; n = 13 cells) that did not colocalize with the ER membrane protein calnexin. To facilitate ATZ immunofluorescence, we constructed ATZ conjugated to Myc and GFP tags in addition to the HA tag. ATZ with each individual tag had similar distribution in Hepa 1-6–transfected cells (Supplemental Figure S1). In the human hepatoma Huh-7 cell line, ATZ had a predominant distribution in the ER and IBs at 24 and 48 h after transfection, respectively (Supplemental Figure S2), consistent with the data of Figure 1A. Others have shown that ATZ and calnexin colocalize in the ER (Teckman and Perlmutter, 2000). The results shown here indicate that although this is the case for a population of transfected cells that had ATZ in a reticular pattern, ATZ segregates in a time-dependent manner to IBs that showed up as different organelles from the main calnexin-containing ER. To determine whether the antibody used in this study labels the ER, cells were transfected with calnexin-GFP. The distribution of GFP fluorescence and calnexin immunostaining was similar (Figure 1C). This shows that the calnexin immunostaining of Figure 1A reflects the actual distribution of the protein.

Differently from ATZ, AAT fluorescence seemed to be concentrated in the Golgi compartment at 48 h (Supplemental Figure S3). This is consistent with the finding that wild-type AAT is efficiently secreted, whereas ATZ is retained inside the cell (Perlmutter, 2002b). When transiently transfected Hepa 1-6 cells were observed by TIRFM, ATZ showed up as a reticular pattern (Figure 1D, bottom) in addition to the brightly fluorescent IBs (Figure 1D, top, red asterisk). In addition, small, round accumulations of ATZ (Figure 1D, bottom, green arrowheads) were associated to the ATZ-positive tubules (Figure 1D, bottom, blue arrows). This suggests that the mutated protein concentrates in enlarged zones of the ER before its sequestration into the IB.

ATZ is prone to polymerization by a loop-sheet insertion mechanism (Lomas *et al*., 1992). By nondenaturing electrophoresis and Western blot analysis of the cell lysates, ATZ occurred as a 45-kDa band and a more abundant 98-kDa band (Figure 1, E and F). To determine whether the 98-kDa band corresponds to ATZ dimers, we coexpressed HA-ATZ

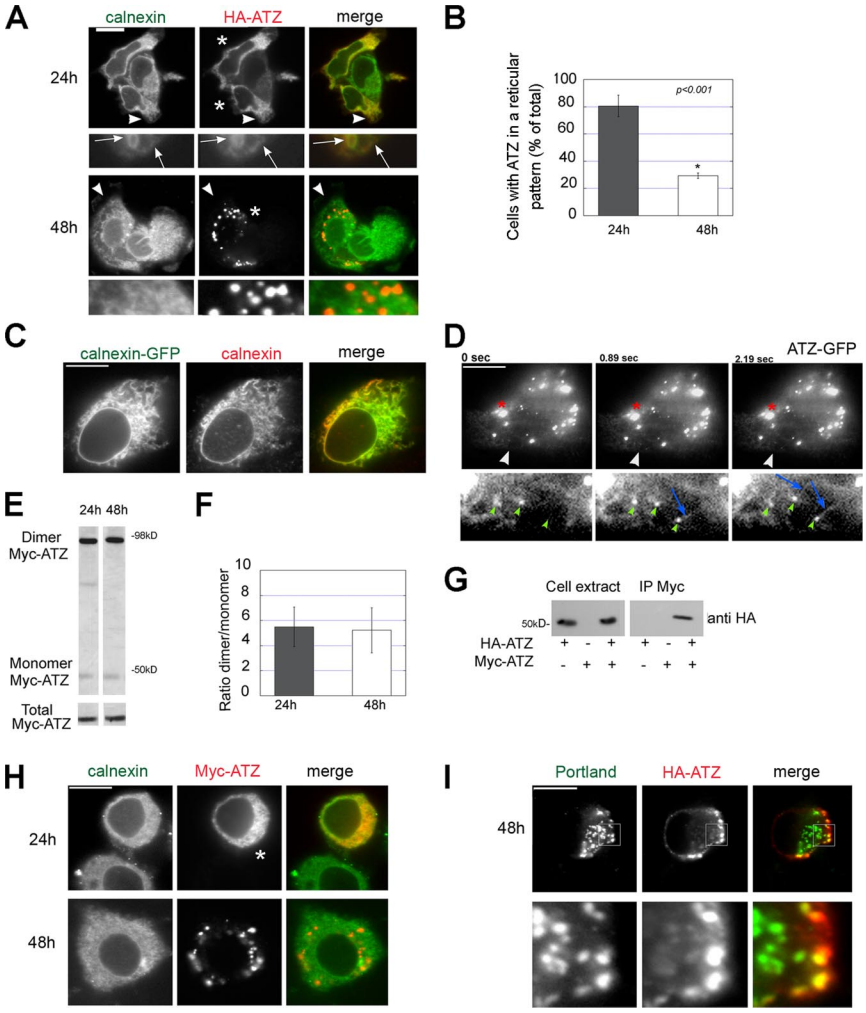

Figure 1. ATZ accumulates in IBs in a time-dependent manner in different cell types. (A) In Hepa 1-6 cells, ATZ localizes to the ER at 24 h after transfection and in IBs 48 h after transfection. Cells were transiently transfected with HA-ATZ-pcDNA3.1 and analyzed by confocal fluorescence microscopy at 24 and 48 h after transfection. Cells were costained with primary rabbit polyclonal antibodies against calnexin to label the ER and mouse monoclonal antibodies against the HA tag. Secondary antibody staining was carried out using FITC-conjugated anti-rabbit antibodies and Cy3-conjugated anti-mouse antibodies. Magnified images (10×) of the regions at the arrowheads are shown in bottom panels. Arrows indicate colocalization of ATZ with calnexin. Asterisks indicate transfected cells. (B) Quantification of cells with ATZ in the ER. To quantify the percentage of cells that have ATZ in the ER, confocal images of 50 cells per time (24 and 48 h) were analyzed. The cells were classified into two groups, either with ATZ in a reticular pattern or with at least one IB. Averages and standard deviations were obtained from the experiment shown in A (n = 50 cells per time). (C) Immunofluorescence images of Hepa 1-6 cells transiently transfected with calnexin-GFP and stained with primary rabbit polyclonal antibodies against calnexin. Secondary antibody staining was carried out using Cy3-conjugated anti-rabbit antibodies. (D) Hepa 1-6 cells were transiently transfected with ATZ-GFP. Approximately 48 h after cell transfection, cells were imaged by TIRFM by using time-lapse acquisition. Bottom, magnified image (10×) of the regions at the arrowheads. Green small arrowheads indicate small round ATZ accumulations at the tip of ATZ-labeled tubules (blue arrows). The red asterisk shows an IB. (E) SDS-page in denaturing (bottom inset) and nondenaturing conditions (top inset) of ATZ cell lysates 24 and 48 h after transfection with Myc-ATZ-pcDNA3.1. Western blots were probed with mouse monoclonal anti-AAT antibody. (F) Averages and standard deviations are derived from three independent samples including that in E. (G) Hepa 1-6 cell lysates were derived from cells transfected with either HA-ATZ-pcDNA3.1, or Myc-ATZ-pcDNA3.1, or both, as indicated. Immunoprecipitations from cell lysates were carried out with anti-Myc antibodies. Immunoprecipitated samples were analyzed by Western blot by using POD-labeled anti-HA antibody. (H) In neuroblastoma N2A cells ATZ localized to the ER and accumulated in IBs at 24 and 48 h after cell transfection, respectively. Confocal microscopy of N2A cells transiently transfected with Myc-ATZ-pcDNA3.1. Cells were costained with rabbit polyclonal antibodies against calnexin and with mouse monoclonal antibodies against the Myc-tag. Secondary antibody staining was carried out using FITC-conjugated anti-rabbit antibodies and Cy3-conjugated anti-mouse antibodies. Asterisks indicate transfected cells. (I) Neuroserpin Portland colocalizes with ATZ. N2A cells were cotransfected with HA-ATZ-pcDNA3.1 and neuroserpin Portland-pcDNA3.1. Confocal microscopy of cells stained with rabbit polyclonal antibodies against neuroserpin and mouse monoclonal anti-HA antibody. Secondary antibody staining was done as in A. Bottom, magnified image (5×) of a region (square) in the top panel. Bars, 25 μm.

and Myc-ATZ (Figure 1G). Anti-Myc antibodies coimunoprecipitated HA-ATZ, indicating that the mutated proteins form dimers and, perhaps, higher polymers. In the cell homogenates, both the amount of ATZ and the ratio ATZ dimer/ATZ monomer remained constant at the 24- and 48-h time points (Figure 1F). These data indicate that formation of IBs is a time-dependent cell response that is not due to changes of either the amount of ATZ at steady state or to increased formation of ATZ polymers.

Portland Neuroserpin Localizes to IBs in Neuroblastoma Cells

To determine whether IB formation is cell specific, we transiently expressed ATZ in N2A cells, and we monitored the distribution of ATZ in respect to that of the ER at 24 and 48 h after cell transfection (Figure 1H). Similarly to the Hepa 1-6 cells, most of the N2A cells formed IBs at the 48-h time point. This shows that the time-dependent IB formation is not specific to the hepatocyte. Diseases due to the accumulation of misfolded proteins have been also reported for other variants of the serpin family (Davis *et al.*, 1999; Miranda *et al.*, 2004). The disease familial encephalopathy with expression of polymerogenic neuroserpin variants leads to dementia, possibly by accumulation of mutant neuroserpins in neurons. The most severe form of dementia is caused by the Portland mutation (S52R) (Carrell, 2005). To determine whether Portland neuroserpin is accumulated in the same compartment as ATZ, the two proteins were coexpressed in neuroblastoma N2A cells. Some of the neuroserpin puncta (31.8% ± 24.7; n = 10 cells) colocalized with ATZ, indicating that at least a fraction of neuroserpin accumulates in IBs (Figure 1I).

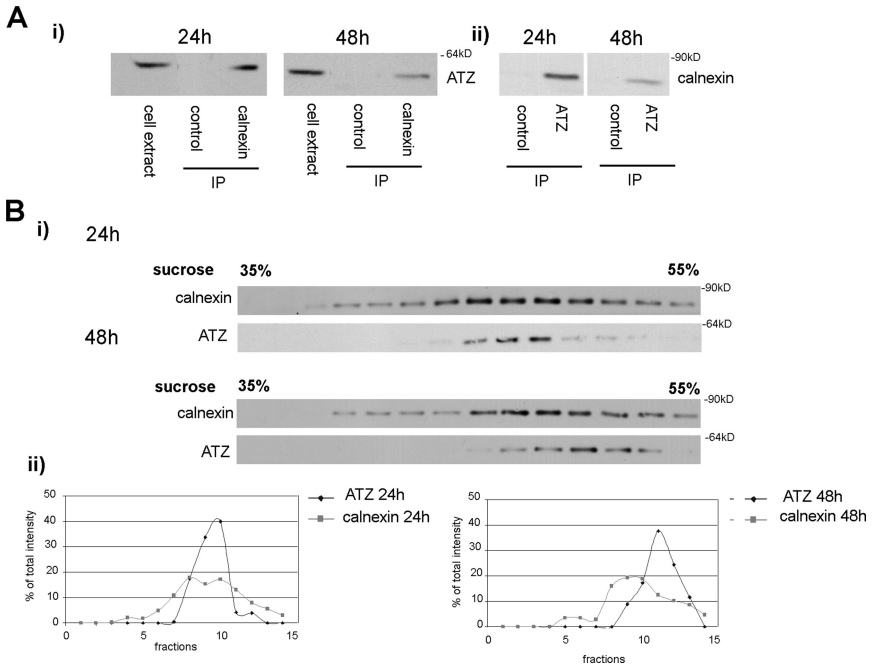

Figure 2. ATZ migrates as a separate peak from calnexin-containing ER in a sucrose density gradient. (A) Decreased binding of ATZ to calnexin at the 48 h compared with the 24-h time points. i, immunoprecipitations of lysates derived from Hepa 1-6 cells expressing ATZ-GFP were carried out without (control) and with calnexin antibody. Immunoprecipitates were analyzed by Western blot by using mouse monoclonal antibodies against AAT. ii, immunoprecipitations of the same samples were carried out without (control) and with AAT antibody. Immunoprecipitates were analyzed by Western blot by using rabbit polyclonal antibodies against calnexin. (B) Twenty-four and 48 h after tranfection of Hepa 1-6 cells with ATZ-GFP, postnuclear supernatants were collected and loaded in parallel onto sucrose density gradients. Fractions were analyzed by Western blot by using antibodies against AAT and calnexin.

ATZ in the IBs Is Sequestered from the Main ER

The ER chaperone calnexin binds ATZ in the ER (Cabral *et al*., 2002). At 48 h after transfection ATZ-containing IBs showed up as a distinct compartment from the main ER labeled by calnexin (Figure 1A). Immunoprecipitation experiments carried out with antibodies against calnexin and AAT showed that at 48 h, the interaction between ATZ and calnexin decreased by ~50% compared with that at 24 h (Figure 2A, i and ii, respectively). Thus, formation of the IBs correlates with decreased ATZ in a complex with calnexin. ATZ-containing IBs might exist as separate organelles from the main ER. In this case, it is possible that the two compartments, ER and IBs, fractionate differently. When PNS derived from Hepa 1-6 cells at 24 h after ATZ transfection was centrifuged onto a sucrose density gradient, the peak of ATZ colocalized with that calnexin (Figure 2Bi). At 48 h after transfection, the peak of ATZ was shifted from that of calnexin, indicating that at least a fraction of ATZ localizes to a compartment separate from the main ER. In the 48-h gradient, the fraction of ATZ migrating together with calnexin may reflect ATZ distribution to the ER in a population of transfected cells (~30%; Figure 1B). To further explore whether IBs are separated from the ER, we used the microtubule-depolymerizing agent nocodazole. Consistent with reports that nocodazole induces the collapse of the ER (Lee *et al*., 1989), incubation of Hepa 1-6 cells with the drug lead to aggregation of calnexin fluorescence into large patches (Figure 3A). At 48 h after transfection, most of the cells had ATZ in the IBs and ATZ fluorescence was separate from the ER patches induced by the drug (Figure 3A, bottom). These data, together with those of Figures 1 and 2, indicate that IBs are organelles distinct from the main ER.

IBs Retain Some ER Components and Are Negative for Autophagosome and Lysosome Markers

Data in Figure 1D suggest that IBs originate from the ER. In this case, unlike calnexin, other ER resident proteins may also be targeted to the IBs. KDEL is a signal sequence required for residency of many proteins in the ER (Pelham, 1996). In untransfected cells, calnexin- and KDEL-containing proteins had similar distribution (Supplemental Figure S4). In transfected Hepa 1-6 cells, KDEL immunoreactivity was both in the ER and concentrated in the IBs, showing that, although separated from the ER, these organelles retain some ER components (Figure 3B, arrowheads). In this respect, it has been reported that ATZ interacts with different cell chaperones that have the KDEL sequence, including PDI and GRP-78/BiP (Schmidt and Perlmutter, 2005; Papp *et al*., 2006). It is possible that these proteins accumulate in the IBs because they bind to ATZ. It has been proposed that a misfolded proinsulin accumulates mainly in ERGIC-53–positive pre-Golgi intermediates, and, to a lesser extent, in the ER (Zuber *et al*., 2004). Thus, ATZ-containing IBs may correspond to pre-Golgi intermediates. To determine whether this is the case, we used human HUH-7 cells that form IBs in response to ATZ expression like the Hepa 1-6 cells (Supplemental Figure S2) and where the intermediate compartment can be labeled by monoclonal antibodies against ERGIC-53 (Schweizer *et al*., 1993). However, ATZ did not colocalize with ERGIC-53, either in the perinuclear localization or in scattered cytoplasmic vesicles (Figure 3C, bottom). Autophagy has been involved in ATZ degradation (Teckman and Perlmutter, 2000; Kamimoto *et al*., 2006). The process occurs by sequestration of cytosol and organelles within double membrane vesicles, the autophagosomes, which then fuse with the lysosomes (Yorimitsu and Klionsky, 2005). We used the autophagosome marker LC3-GFP (Kabeya *et al*., 2000) to determine whether IBs are autophagosomes. ATZ did not colocalize with LC3-GFP (Figure 3D). Moreover, ATZ did not colocalize with the lysosomal marker LAMP1-GFP (Patterson and Lippincott-Schwartz, 2002) (Figure 3E) or with the dye LysoTracker Red that stains lysosomes (Supplemental Figure S4). This shows that IBs are neither classical autophagosomes nor lysosomes.

To further investigate the nature of the IBs and their relation to the ER, we carried out ultrastructural analysis of ATZ-expressing cells. To this end, Hepa 1-6 cells transfected with ATZ-GFP were sorted by fluorescence-activated cell

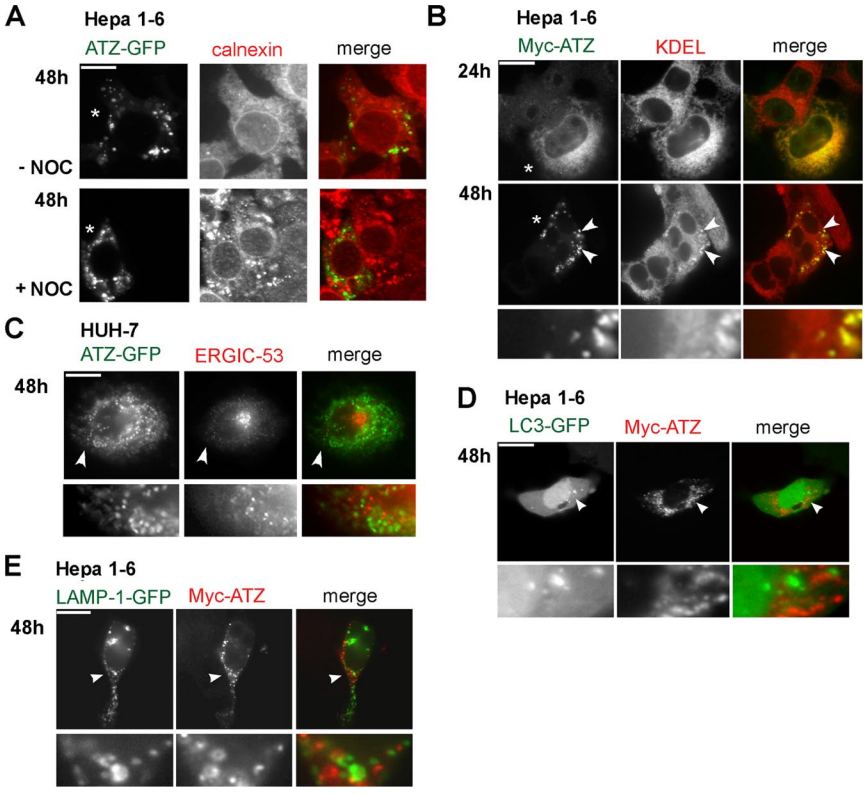

Figure 3. IBs show up as separated from the main ER, do not have autophagosome or lysosome markers, and retain some ER proteins. (A) Treating Hepa 1-6 cells with nocodazole disrupts the ER, and it does not change ATZ distribution in the IBs. Hepa 1-6 cells were transiently transfected with ATZ-GFP and incubated without (−Noc) and with nocodazole (+Noc) at the 48-h times after transfection. Cells were stained with rabbit polyclonal antibodies against calnexin. Secondary antibody staining was carried out using Cy3-conjugated anti-rabbit secondary antibody. Asterisks indicate transfected cells. (B) ATZ in the IBs colocalizes with KDEL sequence-containing proteins. Confocal microscopy of Hepa 1-6 cells transiently transfected with Myc-ATZ-pcDNA3.1. Cells were costained with rabbit polyclonal antibodies against the Myc-tag and the mouse monoclonal antibodies against KDEL. FITC-conjugated anti-rabbit and Cy3-conjugated anti-mouse antibodies were used for secondary staining. The lowest panel has a magnified image (6×) of a region (arrowheads) in the top panel. Asterisks indicate transfected cells. (C) ATZ in the IBs does not localize to the ER-to-Golgi intermediate compartment. Huh-7 cells were transfected with ATZ-GFP and stained using primary mouse monoclonal antibodies against ERGIC-53 and secondary Cy3-conjugated anti-mouse antibodies. Bottom, magnified image (4×) of the region indicated by the arrowhead. (D) ATZ in IBs does not colocalize with the autophagosomal marker LC3-GFP. Hepa 1-6 cells were cotransfected with LC3-GFP and Myc-ATZ-pcDNA3.1 and stained using primary mouse monoclonal antibodies against the Myc-tag and secondary Cy3-conjugated anti-mouse antibodies. Bottom, magnified image (6×) of the region indicated by the arrowhead. (E) ATZ in the IBs does not colocalize with the lysosomal marker LAMP1-GFP. Hepa 1-6 cells were cotransfected with LAMP1-GFP and Myc-ATZ-pcDNA3.1 and stained as described in D. Bottom, magnified detail (6×) of the image shown above and indicated by the arrowhead. Bars, 25 μm.

sorting and analyzed by electron microscopy (Figure 4). Mock-transfected Hepa 1-6 cells were analyzed in parallel. At low magnification, the ATZ-expressing cells had fewer intact mitochondria and ER cisternae, and they had more clear vesicles and darker bodies (Figure 4B, white and black arrows, respectively) than the mock-transfected cells (Figure 4A). At higher magnification, the ER of control cells looked like tubules with enlarged tips (Figure 4C, arrows and arrowhead, respectively). In ATZ-expressing cells, ER tubules had a general appearance similar to control cells, but the tips of were more expanded than those in the control cells and they had a clear, electron-light core (Figure 4D, arrows and arrowheads, respectively). The ultrastructure shown here and the TIRFM of Figure 1D indicate that ATZ accumulates to subdomains of the ER. This is in agreement with immunoelectron microscopy studies showing colocalization of ATZ and calnexin in ER membranes (Teckman and Perlmutter, 2000) and immunoelectron microscopy showing that the liver disease-linked genetic variant null Hong Kong (NHK) of AAT localizes to the rough ER and to ER buds (Zuber *et al*., 2007). The numerous electron-light vesicles of ATZ-expressing cells showed up at higher magnification as round structures with no apparent connection with the ER tubules (Figure 4E), limited by only one membrane, and with and without attached ribosomes (Figure 4F, arrows and arrowheads, respectively). These structures are very similar to those described in the liver of PiZZ patients where ATZ was found in marked dilatations of the ER and smooth vesicles (Yunis *et al*., 1976; Hultcrantz and Mengarelli, 1984; Teckman and Perlmutter, 2000). Our electron microscopy (EM) data suggesting that ATZ induces formation of vesicles are in agreement with a recent work showing that NHK concentrates into vesicles other than the ER cisternae (Zuber *et al*., 2007). At higher magnification, most of the darker bodies (Figure 4B, black arrows) seemed to have multiple membranes (Figure 4G), some of which had the same morphological appearance as mitochondrial cristae. This observation is in agreement with previous studies showing mitochondrial injury in the liver of patients expressing ATZ (Teckman *et al*., 2004). In conclusion, data in Figures 1–3 and the EM shown here indicate that ATZ is in a compartment that does not have calnexin and yet maintains some ER components such as ribosomes and luminal ER proteins. These observations suggest that in ATZ-expressing cells, the ER sheds to form ATZ-containing vesicles that are separate from the main compartment. The ultrastructural analysis of the ATZ-expressing Hepa 1-6 cells of Figure 4 also indicates that these cells recapitulate many structural features of hepatocytes from PiZZ patients.

Overexpression of Calnexin Blocks IB Formation in Hepatoma Cells

The aforementioned results indicate that ATZ is exported out the ER into the IB both in hepatoma and neuroblastoma cells. Calnexin has been reported to be a key chaperone in ATZ disposal. Overexpression of calnexin inhibited ERAD of NHK (Oda *et al*., 2003). In addition, it has been proposed that dissociation of ATZ from calnexin is required for ATZ degradation (Cabral *et al*., 2002). We find that at 48 h, in most of the cells ATZ is out of the ER and sequestered into IBs that do not have calnexin. We reasoned that calnexin association to ATZ might control the formation of IBs by retaining the

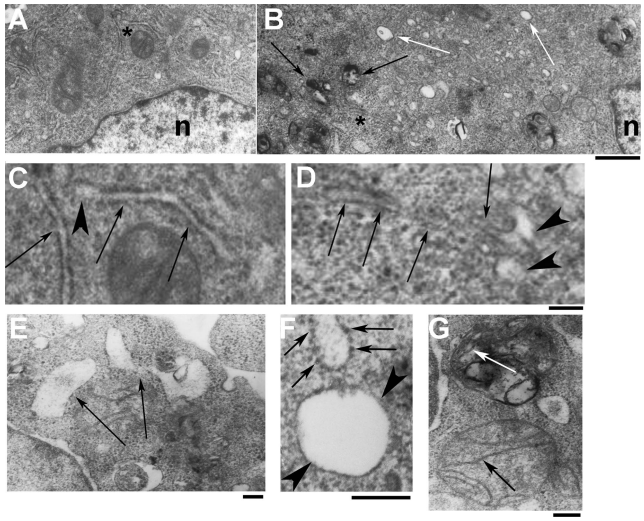

Figure 4. Ultrastructural analysis of Hepa 1-6 cells expressing ATZ. (A and B) Micrographs of control cells (A) and ATZ-expressing cells (B) at the same magnification. B, white arrows and black arrows indicate electron-light and electron-dense organelles. Bar, 1 μm; n, nucleus. (C and D) The fields indicated by the asterisks in the control (A) and ATZ-expressing cells (B) are shown at higher magnification in C and D, respectively. Arrows in C and D indicate the ER; arrowheads indicate the tips of ER cisternae. Bar, 200 nm; C and D are at the same magnification. (E–G) Micrographs of ATZ expressing cells. Bars, 200 nm. Large electron-light bodies limited by one membrane (arrows) are shown in E. A vesicle with attached ribosomes is shown in F (arrows) next to another one without ribosomes (arrowheads). A mitochondrium is shown in G with intact cristae (black arrow) next to an electron-dense body where disrupted cristae are still visible (white arrow).

mutated protein in the main ER. To determine whether this is the case, we cotransfected calnexin and ATZ in the Hepa 1-6 cells. For the analysis, we selected a population of cotransfected cells where calnexin level was increased by approximately twofold at the 48-h time point (n = 40 cells), and we compared these cells to randomly chosen cells transfected with ATZ alone (n = 40 cells; Figure 5, A and B). Overexpression of calnexin shifted ATZ from the IBs to the ER, as indicated by the fourfold increase of ATZ colocalization with the chaperone (Figure 5, B and C). These results show that calnexin is involved in IB formation, and they suggest that release of ATZ from the chaperone is necessary for exit of the protein from the ER. To further investigate this possibility, we determined by immunoprecipitation experiments whether overexpression of calnexin increases binding of ATZ to the chaperone (Figure 5D). Transfection with exogenous calnexin did not induce a significant increase of the chaperone in the population of Hepa 1-6 cells (1.2 $\pm$ 0.35-fold; Figure 5Dii). Note that the measured calnexin level in cell transfected with the exogenous chaperone is lower than that reported in Figure 5A because the general cell population, rather than a selected group of cells as in Figure 5A, was used for the analysis. This is consistent with the observation that only a small percentage of cells is transfected (<20% of the general cell population). It has been reported by others that increased calnexin levels inhibit degradation of the NHK variant of AAT (Oda *et al*., 2003). However, changes of ATZ levels in the population of cells cotransfected with calnexin were again nondetectable compared with cells transfected with ATZ alone (1.2 $\pm$ 0.23-fold; Figure 5Dii). This is probably due to the low cotransfection rate of ATZ with calnexin (<38%). Immunoprecipitation with antibodies against calnexin lead to a sharp increase (5.3 $\pm$ 1.87-fold; Figure 5Di) of coimmunoprecipitated ATZ in samples from cells that were cotransfected with exogenous calnexin compared with those from cells transfected with ATZ alone. Note that the amount of immunoprecipitated calnexin in both samples is the same (Figure 5Di). This indicates that overexpression of the chaperone in the population of cotransfected cells leads to increased interaction of calnexin with ATZ. Together, the results of Figure 5, A and D, indicate that relocation of ATZ to the ER in the presence of overexpressed calnexin is dependent on lack of dissociation of ATZ from the chaperone. These data and those of Figure 2A indicate that release of ATZ from the chaperone is necessary for its exit from the main ER into the IBs.

Overexpression of PDI Does Not Inhibit Formation of IBs

Like in the hepatoma cells, overexpression of calnexin in the N2A cells induced a shift of ATZ distribution from the IBs to the ER (Figure 5, E and F). Therefore, the effect of increased calnexin on ATZ distribution is not cell type specific. It has been reported that in addition to calnexin, ATZ interacts with a variety of other ER chaperones, including PDI (Schmidt and Perlmutter, 2005). Moreover, overexpression of PDI in human embryonic kidney 293 cells inhibits NHK disposal (Hosokawa *et al*., 2006). In addition to the inhibition of ATZ degradation reported by others (Oda *et al*., 2003), we find that increased calnexin blocks IB formation. These observations raise the question as whether different cell chaperones have the same effect on ATZ levels and ATZ cell distribution. We measured the increase of intracellular ATZ in N2A cells in response to PDI and calnexin overexpression. In agreement with previous data, overexpressed PDI increased ATZ levels (Figure 5G). However, calnexin overexpression increased more effectively than that of PDI the cell level of ATZ (by 5.96-fold; $p < 0.0001$; Figure 5G). Next, we measured whether ATZ redistributed to the ER in the presence of increased PDI. IBs are defined as individual organelles of ~2-μm^2 area. ATZ, when localized in the endoplasmic reticulum, occupies a larger area than when the protein is in the IBs (Figure 5E). We reasoned that localization to organelles with an average area of <5 μm^2 would discriminate ATZ in the IBs from that in the ER. Overexpression of calnexin shifted ATZ distribution from IBs to the larger main ER compartment (average area of 2.56 $\pm$ 1.42 and 19.89 $\pm$ 11.9 μm^2, respectively; $p < 0.0001$; Figure 5, E and I). Differently, when PDI was overexpressed, ATZ remained in organelles with the same average area as the control (2.17 $\pm$ 1.64 and 2.65 $\pm$ 1.82 μm^2; Figure 5, H and I). Moreover, PDI localized into the IB together with ATZ (Figure 5H), in agreement with our previous results that these organelles have some ER lumen components (Figure 3B). Thus, unlike calnexin, overexpression of PDI did not inhibit formation of IBs. These data show that calnexin has a specific role in IB biogenesis. Because expression of calnexin increased the amount of ATZ, it is possible that formation of the IBs is one route of ATZ disposal.

Formation of ATZ-containing IBs Occurs in Cells Capable of a Classical Autophagy Response

It has been reported that ATZ expression induces autophagy in the liver of patients and of transgenic mice but not in cells transiently expressing the protein (Teckman *et al*., 2000, 2004; Teckman and Perlmutter, 2000; Kamimoto *et al*., 2006). We reasoned that formation of the IBs or retention of ATZ in the ER induced by increased calnexin levels might result

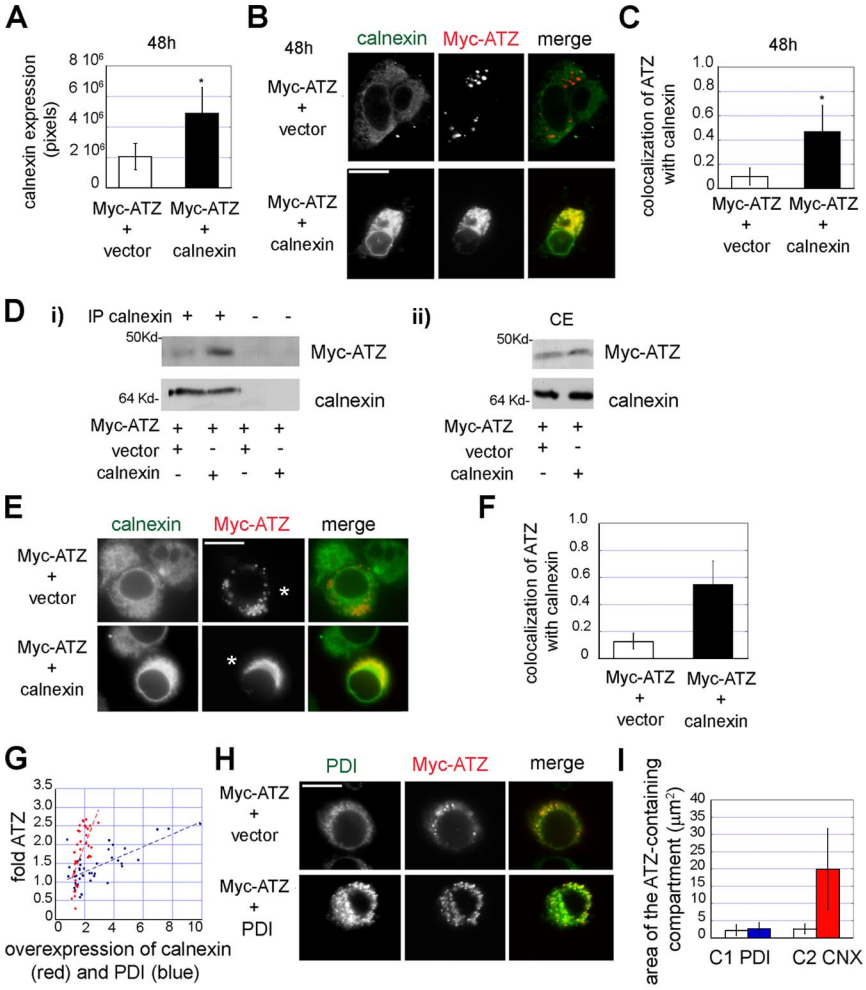

Figure 5. Calnexin and not PDI, controls formation of IBs. (A) Hepa 1-6 cells were cotransfected with Myc-ATZ-pcDNA 3.1 and either empty pcDNA3.1 vector or calnexin-pcDNA3.1, as indicated. In the transfected cells, the levels of calnexin (averages and standard deviations) are derived from 40 cells per condition at the 48 h time. (B) Confocal images showing the shift of ATZ labeling from IBs to the ER in Hepa 1-6 cell without (top) and with exogenous calnexin (bottom), 48 h after cell transfection. Cells were costained with primary mouse monoclonal antibodies against the Myc-tag and rabbit polyclonal antibodies against calnexin. Secondary antibody staining was carried out using Cy3-conjugated anti-mouse and FITC-conjugated anti-rabbit antibodies. (C) Increased colocalization of ATZ with calnexin at the 48-h time in cells overexpressing calnexin (n = 40) compared with the control with endogenous calnexin (n = 40). (D) Cell lysates were derived from Hepa 1-6 cells transfected with either Myc-ATZ-pcDNA3.1 and empty pcDNA3.1 (vector) or cotransfected with Myc-ATZ-pcDNA3.1 and calnexin-pcDNA3.1 48 h after transfection. Immunoprecipitations were carried out without and with rabbit polyclonal anti-calnexin antibodies, as indicated. Immunoprecipitates and cell lysates (CE) were analyzed by Western blot by using mouse monoclonal anti-Myc and rabbit polyclonal anti-calnexin antibodies. (E) In N2A cells increased calnexin levels lead to a shift of ATZ distribution from IBs to the ER. N2A cells were cotransfected with Myc-ATZ-pcDNA3.1 and either empty pcDNA3.1 vector (top) or calnexin-pcDNA3.1 (bottom). For confocal microscopy, cells were costained as described in B. Asterisks indicate transfected cells. (F) Increased colocalization of ATZ with calnexin in cells overexpressing calnexin (n = 30) compared with the control without exogenous calnexin (n = 30) at the 48-h time. (G) Cells were cotransfected with Myc-ATZ-pcDNA3.1 and either PDI-pCMV-SPORT6 or calnexin-pcDNA3.1. The graph shows levels of intracellular ATZ (-fold ATZ) in individual cells overexpressing either calnexin (n = 34) or PDI (n = 41). (H) Confocal images of N2A cells cotransfected with Myc-ATZ-pcDNA3.1 and either empty pcDNA3.1 vector (top) or PDI-pCMV-SPORT6 (bottom). Cells were costained with primary mouse monoclonal anti-PDI and rabbit polyclonal anti-Myc antibodies. Secondary staining was carried out using FITC-conjugated anti-mouse and Cy3-conjugated anti-rabbit secondary antibodies. (I) N2A cells were transfected as described in G. The graph shows the area of the ATZ containing compartment in cells with ATZ alone (C1; n = 15) or with ATZ + exogenous PDI (PDI; n = 15) or with ATZ alone (C2; n = 15) and ATZ + exogenous calnexin (CNX; n = 15). Bars, 25 μm.

from a general inability of the hepatoma cells to activate the autophagy pathway. To monitor induction of autophagy, hepatoma cells were transfected with the autophagosomal marker LC3-GFP (Kabeya *et al.*, 2000). Amino acid starvation is a classical stimulus to induce autophagy (Pattingre *et al.*, 2005). On cell starvation, LC3-GFP changed its distribution with increased formation of "dot-like" autophagosomes in the cytoplasm as described by others (Mizushima *et al.*, 2004; Pattingre *et al.*, 2005) (Figure 6A). Conversely, the number of LC3-GFP–labeled autophagosomes did not significantly increase in response to starvation when cells were preincubated with the autophagy inhibitor 3-methyladenine (Teckman and Perlmutter, 2000) (Figure 6A). When Hepa 1-6 cells expressing either ATZ or ATZ and exogenous calnexin were starved, the number of LC3-GFP–labeled autophagosomes increased similarly to mock-transfected cells (Figure 6, B and C). In cells where autophagy was induced virtually none of the IBs had associated the autophagosome marker LC3-GFP in agreement with the data of Figure 3D. These experiments show that ATZ localization to IBs or ATZ retention in the ER induced by increased calnexin are not caused by lack of autophagy. Incubation of Hepa 1-6 cells expressing ATZ in the absence and in the presence 3-methyladenine did not change either the number of IBs (11.57 ± 11.76 and 12.69 ± 7.8, respectively) or their size (2.19 ± 2.36 and 2.78 ± 2.84 μm^2, respectively). These data indicate that IBs and autophagosomes belong to two different pathways.

Inhibition of IB Formation by Calnexin Overexpression Induces Cell Shrinkage and Impairs the Secretory Pathway

It is not known whether ATZ localization to IBs is toxic or protective to the cell. Because we find that increased calnexin levels impairs exit of ATZ from the ER to IBs, we used this as a tool to determine the role of IBs formation in cell toxicity. When ATZ was retained in the ER in response to increased levels of calnexin, cells seemed smaller than in controls with ATZ localized to the IBs (Figure 7A, i, compare upper and lower panels). In addition to the block of IB formation observed here, overexpression of calnexin inhibits degradation of ATZ with increased cellular levels of the serpin (Oda *et al.*, 2003; Figure 5G). Thus, increased total amount of ATZ, rather than a change in ATZ distribution might induce cell shrinkage. To eliminate effects due to

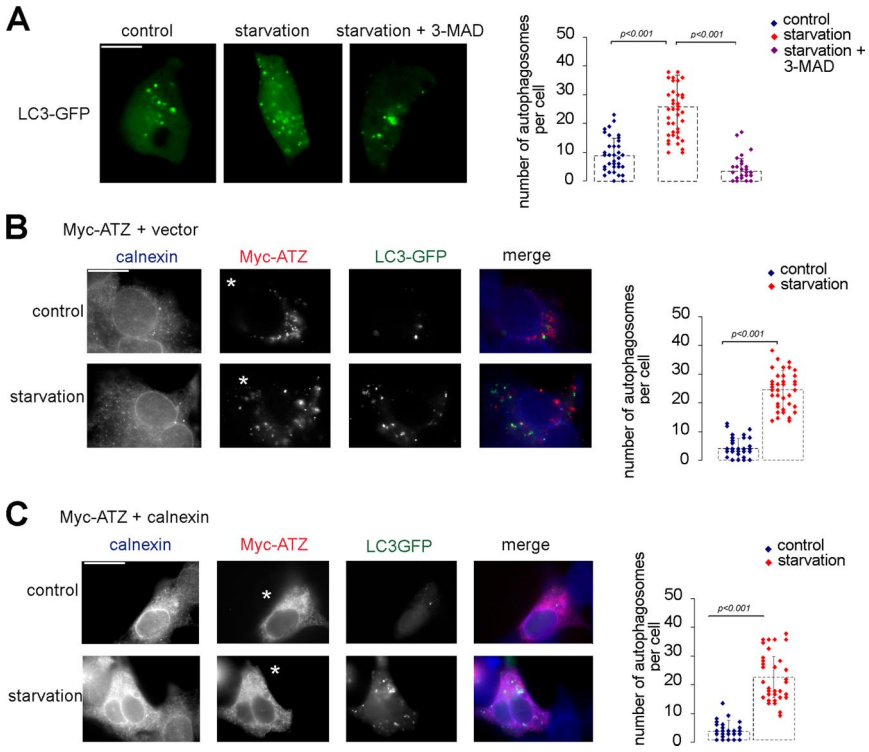

Figure 6. Hepa 1-6 cells are capable of a classical autophagy response. (A) Amino acid deprivation induces autophagy in Hepa 1-6 cells. Cells were transiently transfected with LC3-GFP. Induction of autophagy was inhibited by using 3-methyl-adenine (MAD). Averages and standard deviations shown in the graph were obtained from the experiment in the left panel (n = 45). (B) LC3-GFP does not localize to IBs when autophagy is induced. Hepa 1-6 cells were cotransfected with Myc-ATZ-pcDNA3.1 and LC3-GFP. Immunostaining was done using the rabbit polyclonal antibody against calnexin and mouse monoclonal against the Myc-tag. Secondary staining was carried out using Cy5-conjugated anti-rabbit and Cy3-conjugate anti-mouse antibodies. Averages and standard deviations shown in the graph were obtained from the experiment in the left panel (n = 45). Asterisks indicate transfected cells. (C) Inhibition of IB formation by calnexin overexpression occurs in cells capable of autophagy. Hepa 1-6 cells were cotransfected with Myc-ATZ-pcDNA3.1, calnexin-pcDNA3.1, and LC3-GFP. Immunostaining was done as described in B. Averages and standard deviations shown in the graph were obtained from the experiment in the left panel (n = 45). Asterisks indicate transfected cells.

different levels of ATZ on the cell size, we measured the area of cells that had similar amounts of mutated serpin either with or without increased calnexin (ATZ = $1.10 \pm 0.49 \times 10^6$ and $1.33 \pm 0.53 \times 10^6$ pixels, respectively). Cells were stained to visualize at the same time calnexin, ATZ, and F-actin, and the cell margins were drawn manually on the merged image (Figure 7A). The mean area of the Hepa 1-6 cells transfected with ATZ was not significantly different from that of cells cotransfected with AAT and exogenous calnexin (406.25 ± 104.48 and 377.07 ± 122.27 μm^2, respectively; Figure 7, A and B). This shows that when ATZ is in the IBs, cells have normal shape. In contrast, cells transfected with ATZ and exogenous calnexin had a size that was approximately half (203.49 ± 74.74 μm^2) of that of cells transfected with ATZ alone. This shows that block of IB formation and retention of ATZ in the ER causes cell shrinkage.

It is possible that the accumulation of ATZ in the ER induced by increased levels of calnexin leads to impaired ER function with reduced flow of proteins along the secretory pathway. To determine whether this is the case, hepatoma cells were transfected with proinsulin-pcDNA3.1. In these cells, proinsulin was constitutively secreted as an unprocessed prohormone (Figure 7C). Cells that were cotransfected with both the proinsulin and ATZ plasmids had a rate of prohormone secretion that was reduced to 74.80 ± 5.05% ($p < 0.05$) of that of control cells transfected with proinsulin alone. This indicates that expression of the mutated serpin inhibits constitutive exocytosis. When cells were cotransfected with the proinsulin, ATZ, and calnexin plasmids, the rate of prohormone secretion was further reduced to 60.6 ± 2.74% ($p < 0.005$) of the control cells transfected with proinsulin alone. Conversely, in the absence of ATZ, cotransfection of calnexin together with proinsulin did not change the rate of prohormone release compared with control cells transfected with proinsulin alone. Thus, it seems that elevated calnexin further impairs (by 18.9%; $p < 0.02$), a secretory pathway that is already made less efficient by expression of ATZ.

To further explore the possibility that increased calnexin impairs constitutive secretion, we used endocrine cells that have both the constitutive and regulated secretory pathway. Unlike the constitutive pathway where proteins are constantly secreted, the regulated pathway stores proteins into organelles such as hormone-containing granules. This allows us to visualize directly proteins that have already traversed the ER, exited the *trans*-Golgi network, and are in granules poised for secretion. N2A cells have dense core granules at the tip of neurite-like processes where hormones are stored (Chevrier *et al.*, 1991; Baldini *et al.*, 2005). Expression of proinsulin in some endocrine cells other than the islet β-cells leads to targeting of mature insulin to dense core granules (Moore *et al.*, 1983). To determine whether proinsulin is processed to the mature hormone in the N2A cells, we measured the amount of insulin and proinsulin by ELISA in transiently transfected Hepa 1-6 and N2A cells. In the Hepa 1-6 and N2A cell lysates the amount of proinsulin was comparable with 11.63 and 4.5 pmol/10^6 cells, respectively. In contrast, insulin was almost undetectable in the Hepa 1-6 cells compared with the N2A cells with 2.10 and 70.92 mU/10^6 cells of the mature hormone, respectively. This indicates that a fraction of the prohormone is converted to the mature form in the N2A cells. Insulin immunoreactivity in N2A cells occurred in a Golgi-like compartment near the nucleus and as punctuate staining at the tips of neurite-like processes and colocalized with the granule-associated protein Rab3A (data not shown) (Martelli *et al.*, 2000). This indicates that N2A cells process proinsulin to its mature form and store it in dense core granules. Having established targeting of insulin to the granules in the N2A cells, we asked whether the redistribution of ATZ to the ER induced by increased calnexin levels blocked insulin traffic to the granules. In cells coexpressing ATZ and proinsulin,

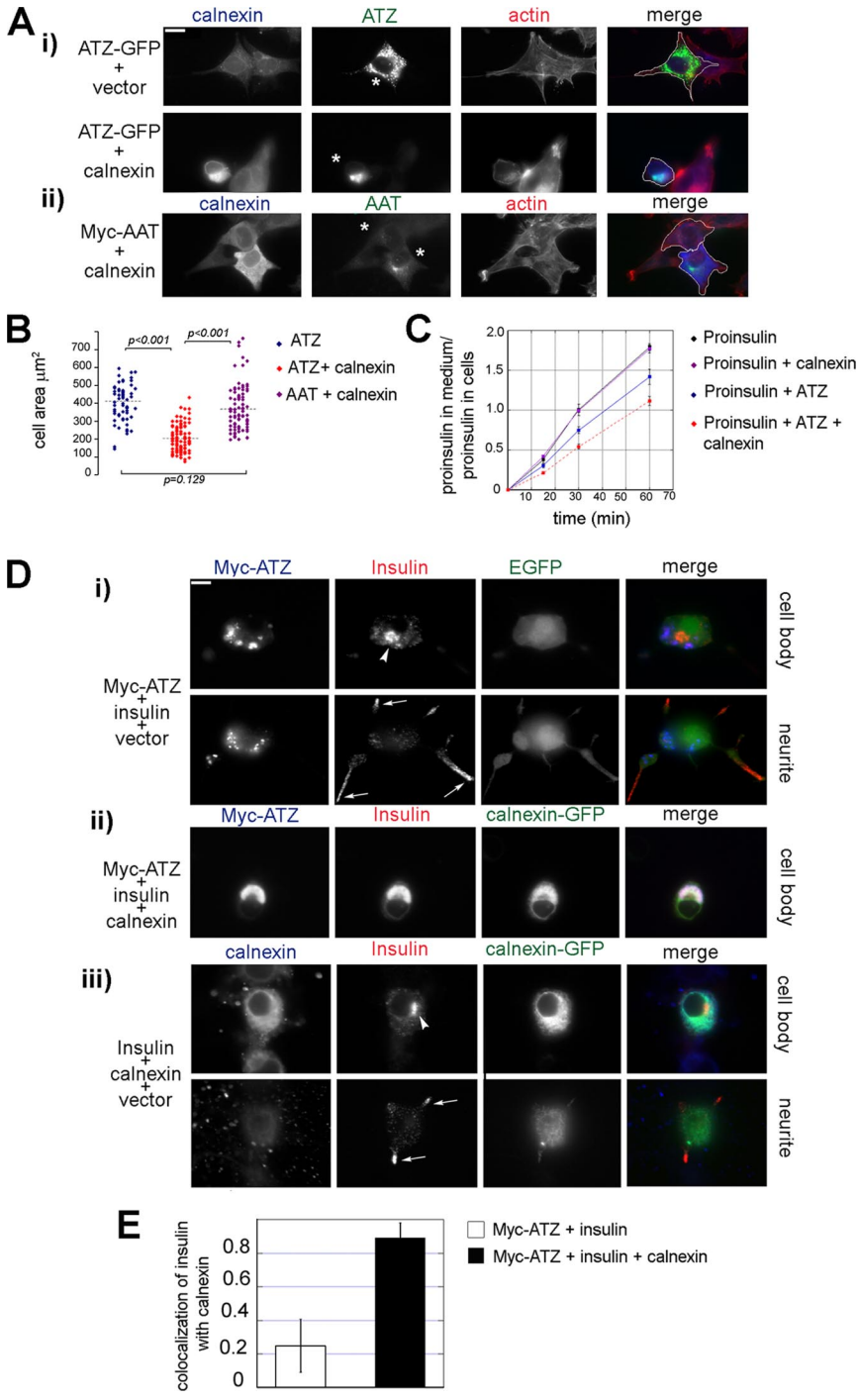

Figure 7. Inhibition of IB formation causes shrinkage in Hepa 1-6 cells and impairs constitutive exocytosis. (A) Increased levels of calnexin induce cell shrinkage in ATZ expressing cells. i, cells were cotransfected with ATZ-GFP and either empty pcDNA3.1 vector or calnexin-pcDNA3.1. Cells were costained with antibodies against calnexin and with the F-actin binding dye Alexa Fluor-Phalloidin. Secondary antibody staining was carried out using Cy5-conjugated anti-rabbit secondary antibodies. ii, Hepa 1-6 cells were cotransfected with Myc-AAT-pcDNA3.1 and calnexin-pcDNA3.1. Staining was done using rabbit polyclonal anti-calnexin and mouse monoclonal anti-Myc antibodies and Alexa Fluor-Phalloidin. Secondary staining was carried out using Cy5-conjugated anti-rabbit antibodies and FITC-conjugate anti-mouse. Asterisks indicate transfected cells, and cell outlines are traced in the merged image following the F-actin staining. (B) Area of cells expressing ATZ-GFP (n = 63), ATZ-GFP and exogenous calnexin (n = 105), and Myc-AAT and exogenous calnexin (n = 86). Calnexin overexpression was calculated by the following ratio: total pixel intensity of calnexin (blue channel) in transfected cells/total pixel intensity of calnexin (blue channel) in the neighboring nontransfected cells (n = 3 for each transfected cell). Overexpression of calnexin in the group of cells expressing ATZ and exogenous calnexin was 2.02 ± 0.83 and in the group of cells expressing AAT and exogenous calnexin was 2.32 ± 0.75. (C) Constitutive secretion is profoundly impaired in hepatoma cells coexpressing ATZ and exogenous calnexin. Hepa 1-6 cells were transfected with either proinsulin-pcDNA3.1 or with proinsulin-pcDNA3.1 and calnexin-pcDNA3.1, or with proinsulin-pcDNA3.1 and ATZ-GFP or with proinsulin-pcDNA3.1, ATZ-GFP and calnexin-pcDNA3.1, as indicated. Proinsulin secretion was calculated using the following ratio: proinsulin in the medium (pM)/proinsulin in the cell lysate (pM). (D) Overexpression of calnexin in ATZ-expressing cells blocks the secretory pathway at the ER level. Epifluorescence images were taken 48 h after cell transfection. i, N2A cells were cotransfected with Myc-ATZ-pcDNA3.1, proinsulin-pcDNA3.1, and empty GFP vector. Cell body and neurites were visualized at two focal planes as indicated. Insulin localizes in a Golgi-like compartment (arrowhead) and to dense core granules at the tips of the neurites (arrows). Cells were costained with the mouse monoclonal antibodies against the Myc-tag and rabbit polyclonal antibodies against insulin. Secondary staining was done with Cy5-conjugated anti-mouse and Cy3-conjugated anti-rabbit antibodies. ii, N2A cells were cotransfected with Myc-ATZ-pcDNA3.1, proinsulin-pcDNA3.1, and calnexin-GFP. Cells were costained as described in i. iii, N2A cells were transfected with proinsulin-pcDNA3.1, empty pcDNA3.1 vector, and calnexin-GFP. Cells were costained with the mouse monoclonal anti-insulin and the rabbit polyclonal anti-calnexin. Secondary staining was done with Cy3-conjugated anti-mouse and the Cy5-conjugated anti-rabbit antibodies. Insulin localized to the Golgi-like compartment (arrowhead), and to dense core granules at the tip of the neurite (arrows) as shown in i. (E) Colocalization of ATZ with insulin is increased in the cells overexpressing calnexin (n = 30) compared with the control (GFP) with ATZ alone (n = 30). Averages and standard deviations are derived from the experiment shown in D. Bars, 25 μm.

ATZ was in the IBs, and insulin immunoreactivity was evident in granules at the tips of the processes (Figure 7Di, bottom, arrows) and in the Golgi-like compartment (Figure 7Di, top, arrowhead), with little colocalization of the two proteins. This indicates that, when ATZ is localized to the IBs, proinsulin traverses the ER and the mature hormone is targeted to the granules. Differently, in N2A cells that coexpressed proinsulin together with ATZ and calnexin, the

insulin immunoreactivity was retained in the ER together with ATZ as shown by the colocalization of ATZ and calnexin immunofluorescence (Figure 7Dii and E). Insulin-containing granules were not visible. Overexpression of calnexin by itself did not shift insulin distribution from the granule to the ER (Figure 7Diii). These experiments show that failure to sequester ATZ in IBs and consequent accumulation of the mutated ATZ in the ER induces a block in the secretory pathway at the step of protein exit from the ER.

Inhibition of IB Formation in N2A Cells Inhibits Neurite Formation

Neurite extension is a process that occurs by polarized addition of newly synthesized proteins and lipids at the tips of the neurites and requires an intact secretory pathway (Futerman and Banker, 1996). As an additional assay to determine the function of the IBs in the secretory pathway, we asked whether increased levels of calnexin blocked neurite formation in N2A cells that express ATZ. To measure the neurite outgrowth in ATZ expressing cells with and without exogenous calnexin, we selected cells with the same amount of ATZ (ATZ = $0.64 \pm 0.12 \times 10^6$ and $0.70 \pm 0.16 \times 10^6$ pixels, respectively). Calnexin, ATZ, and F-actin were visualized together (Figure 8A). The percentage of ATZ-expressing N2A cells that had neurites was $49.0 \pm 9.7\%$ (Figure 8Ai and B). This was not significantly different compared with cells expressing AAT and exogenous calnexin with $51.8 \pm 10.2\%$ of cells having neurites (Figure 8Aiii and B). In contrast, coexpression of ATZ and exogenous calnexin, inhibited formation of the neurites with $8.9 \pm 6.3\%$ of cells having the processes (Figure 8Aii, asterisk, and B). These data together with those in Figure 7 indicate that inhibition of IB formation impairs the secretory pathway at the ER level.

Retention of ATZ in the ER Induced by Increased Calnexin Expression Leads to Induction of the UPR

ER stress induces a protective cell response, the UPR, with increased level of ER chaperones. It has been reported that expression of ATZ in the hepatocytes of transgenic mice and cell lines does not lead to a classical UPR with increased levels of ER chaperones (Hidvegi *et al*., 2005). It is possible that the lack of UPR activation in response to ATZ expression is due to segregation of ATZ out of the main ER to the IBs. In this case, retention of ATZ in the main ER in response to elevated calnexin levels might lead to UPR induction. To monitor UPR induction in Hepa 1-6 cells, we used tunicamycin, a drug that inhibits protein *N*-glycosylation and induces ER stress. UPR induction in response to ER stress can be monitored in HeLa cells by the increased levels of the ER chaperone GRP-78/BiP (Okada *et al*., 2002). Exposure of Hepa 1-6 cells to tunicamycin increased GRP-78/BiP immunoreactivity by approximately twofold (Figure 9A, lane 1 and 2), indicating that the drug induced a classical UPR in our experimental conditions. The level of GRP-78 did not change in cells expressing ATZ compared with cells transfected either with calnexin or with vector alone (Figure 9A, compare lanes 4 with lanes 3 and 1). This indicates that expression of ATZ or overexpression of calnexin does not induce the UPR. Conversely, coexpression of exogenous calnexin and ATZ lead to a significant increase of GRP-78 immunoreactivity compared with cells expressing ATZ alone (Figure 9A, lanes 5 and 4), indicating that the shift of ATZ from the IBs to the ER induces the UPR. To determine whether UPR induction occurred in the population of transfected cells, we monitored cells by immunofluorescence microscopy. Unfortunately, the antibody against GRP-78 could not visualize the mouse protein by immunofluorescence. Others have used an antibody against KDEL to monitor UPR induction by measuring increased GRP-78 levels by Western blot analysis (Lee, 2005). Tunicamycin treatment increased KDEL immunoreactivity in the Hepa 1-6 cells (Figure 9B). This indicates that induction of the UPR can be measured by the KDEL antibody by quantitative immunofluorescence microscopy. Expression of ATZ in the IBs did not increase KDEL immunoreactivity in the Hepa 1-6 cells (Figure 9Ci, iii, and v) consistent with the Western blot analysis of Figure 9A. Coexpression of ATZ and exogenous calnexin increased KDEL immunoreactivity by twofold compared with control cells expressing ATZ alone (Figure 9C, iii, iv, and v). We eliminated possible confounding effects due to different levels of ATZ on UPR induction by selecting for the analysis populations of cells with the same amount of ATZ (ATZ = $1.51 \pm 0.66 \times 10^6$ and $1.52 \pm 0.69 \times 10^6$ pixels in cells without or with increased calnexin, respectively). Conversely, a population of cells with no ATZ and similar levels of exogenous calnexin as the cells coexpressing the exogenous chaperone together with ATZ (calnexin = $2.97 \pm 1.37 \times 10^6$ and $3.01 \pm 1.175 \times 10^6$ pixels, respectively) did not have increased KDEL immunoreactivity (Figure 9Cii, iv, and v). In sum, both Western blot analysis and immunofluorescence experiments indicate that segregation of ATZ to the IBs prevents ER stress and the onset of the UPR.

It is possible that formation of the IBs requires an intact ER. To determine whether this is the case, we measured formation of the IBs when ER stress was induced by tunicamycin treatment. Incubation with the drug dramatically decreased IBs formation with ATZ accumulation in the ER (Figure 9D). The data in Figure 9, C and D, suggest that ER stress initiated by other factors than ATZ expression may lead to retention of the mutated serpin in the ER and that this, in turn, may contribute to ER damage.

DISCUSSION

Cell toxicity induced by expression of ATZ and other polymerogenic serpins is classically considered to be due to retention of serpin aggregates in the endoplasmic reticulum (Carrell, 2005; Rudnick and Perlmutter, 2005). In addition, it is known that ATZ and other polymerogenic serpins form aggregates in "globules" or membrane-enclosed IBs in the liver and brain of affected individuals and in transfected cell models. The nature of the serpin-containing IBs in respect to the ER is unclear. Here, it is found that ATZ in the IBs does not have the same distribution as calnexin, an abundant ER chaperone, indicating that ATZ in the IBs is segregated from the main ER. In support of this possibility, IBs occurred in cells that otherwise maintained a largely intact ER, visualized both by the classical reticular pattern of calnexin distribution by fluorescence microscopy and by the overall normal appearance of ER cisternae at the ultrastructural level. It is possible that IBs are specialized ER sites that then develop to form separate organelles. In agreement with the second possibility, we find that microtubule disruption induced the collapse of the ER into structures that are clearly separated from the IBs and that ATZ migrated as a shifted peak from calnexin-containing ER by sucrose density gradient centrifugation. IBs might originate from shedding of the ER to form separate organelles. In this respect, ATZ-expressing cells have both ER tubules with enlarged, electron-light tips and numerous electron-light vesicles that do not maintain connections with the ER tubules. This suggests that ATZ would first concentrate at the tips of the ER cisternae and then form ATZ-containing vesicles that are separate from the ER. In respect to the possibility that IBs originate from the ER,

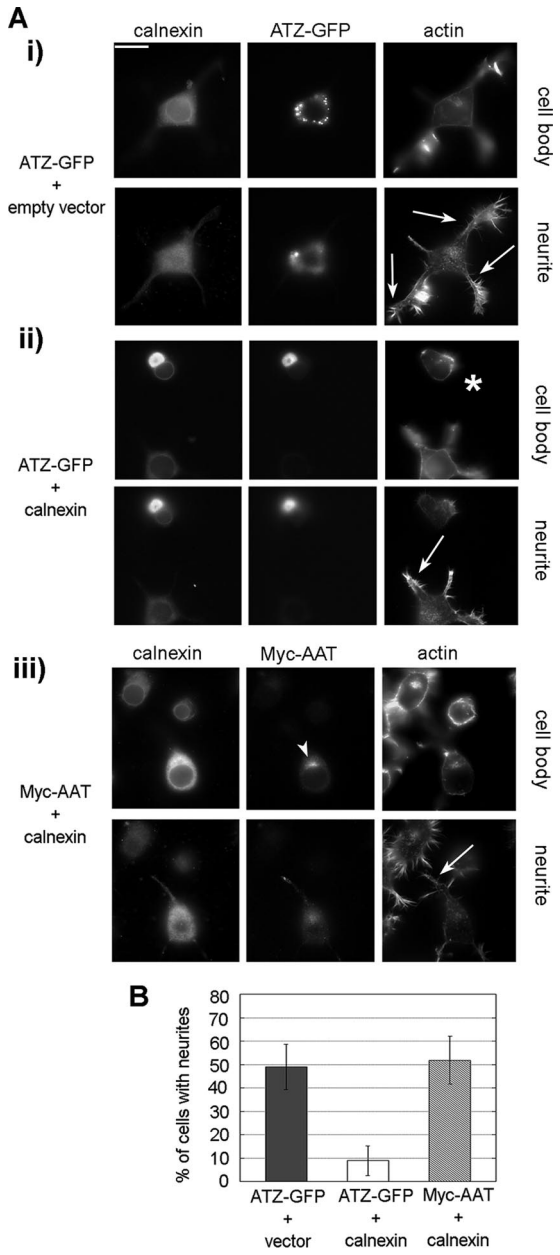

Figure 8. Block of IB formation inhibits neurite outgrow in neuroblastoma cells. (A) Epifluorescence images were taken 48 h after cell transfection. Neurite outgrowth was induced by incubating cells in the absence of serum for 24 h. The two panels represent two different focal planes of the same cell. i, N2A cells were cotransfected with ATZ-GFP and empty pcDNA3.1 vector. Cells were stained with rabbit polyclonal antibodies against calnexin and Alexa Fluor-Phalloidin to label F-actin and visualize neurites (arrows). Secondary staining was carried out using Cy5-conjugated anti-rabbit antibodies. ii, N2A cells were transfected with ATZ-GFP and calnexin-pcDNA3.1. Asterisk, transfected cell; arrows, neurites of nontransfected cells. Cells were stained as described in i. iii, N2A cells were cotransfected with Myc-AAT-pcDNA3.1 and calnexin-pcDNA3.1. Cells were costained with rabbit polyclonal antibodies against calnexin, mouse monoclonal antibodies against the Myc-tag, and Alexa Fluor-Phalloidin. Secondary staining was carried out using Cy5-conjugated anti-rabbit and FITC-conjugated anti-mouse antibodies. Bar, 25 μm. (B) Percentage of N2A cells with neurites in cells expressing ATZ-GFP (n = 54); ATZ-GFP and calnexin (n = 54); and Myc-AAT and calnexin (n = 39). Overexpression of calnexin in the group of cells expressing ATZ and exogenous calnexin was 1.67 ± 0.54 and in the group of cells expressing AAT and exogenous calnexin was 1.87 ± 0.73. Calnexin overexpression was measured as in Figure 7B.

ATZ concentrated in vesicles that could be visualized by TIRFM at the tips of ATZ-containing tubules, whereas there was no colocalization of ATZ with ERGIC-53 a marker of the ER-to-Golgi intermediate compartment (Schweizer *et al.*, 1993). These data are in agreement with a recent observation that vesicles containing another polymerogenic serpin, the NHK variant, bud from the ER (Zuber *et al.*, 2007). IBs, once separated from the ER, may yet retain some ER components such as luminal ER proteins (Figure 2) and ribosomes (Figure 4), as indicated by the rough ER-like ultrastructural appearance of ATZ-induced vesicles visualized both in transfected hepatoma cells (Figure 4) and in liver biopsies from patients with the disease (Yunis *et al.*, 1976; Teckman and Perlmutter, 2000).

The work presented here shows that the ER chaperone calnexin functions in the cell localization of ATZ by controlling traffic of the protein from the ER to the IB. We have defined IBs as organelles of ~2 μm^2 area that do not have calnexin, maintain some other ER components such as the luminal protein PDI, and they are different from autophagosomes and lysosomes. We show that increased expression of calnexin leads to increased association of ATZ to the chaperone, retention of ATZ in the ER, and blocks formation of IBs both in hepatoma and neuroendocrine cells. This indicates that dissociation of ATZ from calnexin is a limiting factor for entry of ATZ into the IB. The role of calnexin in ATZ localization is specific because overexpression of another chaperone, PDI, did not block IB formation. The role of calnexin in ATZ disposal has been described by several studies where it has been reported that dissociation of ATZ from the chaperone is implicated in the degradation pathway of the mutated serpin (Liu *et al.*, 1997, 1999; Cabral *et al.*, 2000; Oda *et al.*, 2003). We did not study the role of calreticulin in ATZ distribution because this soluble calnexin homologue has not been found to interact with the serpin (Cabral *et al.*, 2002). Our work extends the role of calnexin as a regulator of ATZ cell traffic from the ER to IBs. It remains to be determined whether the decrease of ATZ disposal consequent to calnexin overexpression is dependent on inhibition of IB formation.

Another major conclusion of this article is that formation of ATZ-containing IBs is a cell-protective mechanism. In this respect, we find that when ATZ was localized in the IBs, the overall morphology of hepatoma cells was maintained, whereas retention of ATZ in the ER lead to cell shrinkage. Moreover, in hepatoma cells, constitutive exocytosis monitored by the ability of exogenously expressed proinsulin to be secreted in the medium, was more profoundly impaired when ATZ localization shifted from the IBs to the ER. It is possible that reduced flow of proteins and lipids along the secretory pathway impairs the cell ability to maintain a normal shape. However, increased calnexin levels in ATZ-expressing cells seemed to affect more severely the cell morphology than the secretory pathway (Figure 7). In this respect, the entire cell population chosen for the morphological cell shrinkage assay had, together with expressed ATZ, increased calnexin levels, as monitored by quantitative immunofluorescence microscopy. Differently, only a fraction of the insulin-transfected cell population that expressed ATZ had also increased calnexin levels because the rate of cotransfection with the three plasmids was <25%. Thus, it is possible that the different severity of the constitutive secretion and cell shrinkage phenotype is

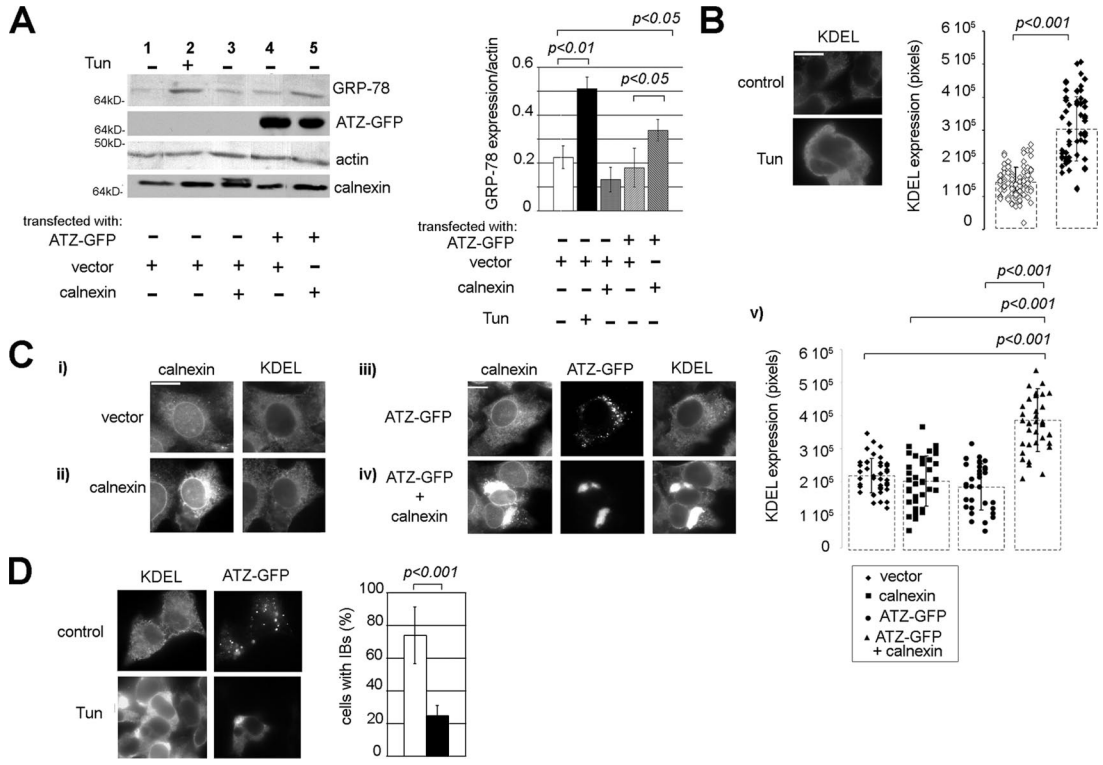

Figure 9. Formation of IBs prevents induction of the UPR. (A) Hepa 1-6 cells were transfected as indicated and treated in the absence and in the presence of tunicamycin (Tun). Cell lysates were analyzed by Western blot by using the indicated antibodies. Right, GRP-78/BiP and actin levels were measured by densitometry. Averages and standard deviations were determined from three independent samples including that shown in the left panel. (B) Tunicamycin increased KDEL immunoreactivity in Hepa 1-6 cells. Left, cell immunostaining was done using the mouse monoclonal antibodies against KDEL. Secondary staining was carried out using Cy3-conjugated anti-mouse antibody. Right, averages and standard deviations of KDEL immunoreactivity were measured by quantitative fluorescence microscopy of 75 cells per condition. Cells were from the experiment shown in the left panel. (C) i and ii, Hepa 1-6 cells were transfected with empty pcDNA3.1 (vector) or with calnexin-pcDNA3.1 and costained with the mouse monoclonal antibodies against KDEL and rabbit polyclonal antibodies against calnexin. Secondary staining was carried out using Cy3-conjugate anti-mouse and Cy5-conjugate anti-rabbit antibodies. iii and iv, cells were transfected with ATZ-GFP and pcDNA3.1 or with ATZ-GFP and calnexin-pcDNA3.1. Cells were stained as described in i. v, graph shows averages and standard deviations of KDEL pixel intensity in cells (n = 45 cells per condition) from the experiment shown in i–iv. (D) Induction of ER stress by tunicamycin inhibits IBs formation. Hepa 1-6 cells were transfected with ATZ-GFP and treated in the absence and in the presence of tunicamycin. Cells were immunostained as described in B. For the quantification shown in the graph, we measured the percentage of cells that had 1 or more IB (n = 100 cells per condition).

due to a lack of exogenous calnexin and ATZ coexpression in the majority of the insulin-secreting cells monitored by the biochemical assay. Another possibility is that other factors besides the efficiency of the secretory pathway modulates cell shape in the ATZ-expressing cells. As an additional model to monitor the effect of ATZ localization on the secretory pathway, we used neuroendocrine cells. In cells with ATZ localized to the IBs, insulin was targeted to dense core granules, whereas ATZ retention in the ER blocked granule formation with accumulation of the hormone in the ER. Furthermore, neurite outgrowth, a process that occurs by membrane apposition of newly synthesized proteins (Futerman and Banker, 1996), occurred normally in neuroendocrine cells expressing ATZ in the IBs and was severely impaired in cells with ATZ in the ER. In sum, these data show that when ATZ is in the IBs the ER function is largely preserved and cell toxicity is limited. In contrast, when the formation of IBs is blocked and ATZ remains in the ER, the secretory pathway is more severely damaged, and cell toxicity is dramatically increased. In sum, in this work cell toxicity is measured by using three parameters, the ability of ER to secrete proteins, the induction of ER stress and maintenance of a normal cell shape. We consider formation of IBs cell protective because, in their presence, ability of proteins to traverse the secretory pathway was less impaired, the UPR was not induced, and cell morphology was maintained. This work has not addressed other long-term aspects of cell protection such as cell viability and outcome of induction of the UPR, nor the effects of IB formation on ATZ degradation. Further studies are required to understand how IB formation determines the cell fate over time. It has been reported that decreased levels of diffuse mutant huntingtin in the cytosol of neurons due to the formation of huntingtin aggregates in IBs reduces cell death (Arrasate *et al*., 2004). Moreover, huntingtin-dependent cell toxicity precedes IB formation (Bennett *et al*., 2005; Diaz-Hernandez *et al*., 2006). Unlike huntingtin, ATZ accumulates in membrane surrounded compartments (Feldmann *et al*., 1974; Yunis *et al*., 1976; Hultcrantz and Mengarelli, 1984; Teckman and Perlmutter, 2000). The data presented here provide the first evidence to the hypothesis that sequestration of misfolded proteins from the secretory pathway to membrane-bound IBs is cell protective.

The UPR is induced by accumulation of unfolded proteins in the ER (Mori, 2003). Differently from other misfolded proteins, expression of ATZ does not seem to induce the

UPR (Hidvegi *et al*., 2005). Results presented in this article suggest that the mutated serpin does not induce the UPR because the protein is either exported out of the ER or segregated to specialized ER locations. In light of our results, we predicted that IB formation blocks induction of the UPR by sequestering the mutated serpin out of the ER. In respect to this, we find that, when formation of the IBs is blocked and ATZ is retained in the ER, the UPR is activated. These observations indicate for the first time that the cell localization of ATZ is a key modulator of the type of cell response induced by expression of the serpin. The UPR is a complex signal transduction response that leads to transcriptional activation of many chaperones including GRP-78/BiP, PDI, calnexin, and calreticulin (Kozutsumi *et al*., 1988; Okada *et al*., 2002; Schroder and Kaufman, 2005; Reyes *et al*., 2006). It is tempting to speculate that the earliest cell response to ATZ expression in the ER is acquisition of the ability to form IBs. In support of this idea, it is found that the number of ATZ-containing IBs is increased at the 48-h time point compared with the 24-h time point after cell transfection with ATZ. At these times, the steady-state amount of total ATZ or ATZ polymers present in the cell remained the same (Figure 1). Thus, ATZ segregation to the IBs seems to be an induced, time-dependent cell response. Failure to form the IBs, as in the case of increased levels of calnexin, may lead to a secondary cell response with activation of the UPR. We also find that when ER stress was induced by tunicamycin, this lead to a block of IBs formation. Together, these data indicate that ER stress has negative effects on the cell ability to segregate ATZ into the IBs. The UPR is generally thought as a cell-protective pathway aimed to reduce the amount of unfolded proteins in the ER. However, in ATZ expression, activation of the UPR coexisted with a more severe disruption of the secretory pathway and increased cell toxicity. It is possible that massive accumulation of ATZ in the ER may overwhelm the UPR and cause loss of ER function. In conclusion, the data presented here indicate lack of ER stress in response to ATZ expression as a direct, and possibly cell-protective, consequence of IBs formation.

Autophagy has been proposed as a major pathway of ATZ degradation. Here, we find that expression of ATZ in hepatoma cells induces formation of IBs that do not have associated LC3, the marker of these organelles. Similarly, in liver from transgenic mice, the ATZ-containing IBs did not colocalize with LC3 (Kamimoto *et al*., 2006). These data indicate that most of the ATZ-containing IBs are not autophagosomes. In contrast, in mouse embryonic fibroblasts expressin dominant-negative Rab7, some ATZ immunoreactivity colocalized with the autophagosome marker (Kamimoto *et al*., 2006). Moreover, inhibitors of autophagy decrease the rate of ATZ degradation, indicating that the process is important for ATZ disposal (Teckman and Perlmutter, 2000). In this respect, IBs may function as an intermediate compartment between the ER and the autophagosomes. However, inhibitors of autophagy, although decreasing the number of autophagosomes in the hepatoma cells, did not change the number or size of IBs. These observations indicate that IBs and autophagosomes belong to different pathways. Our data together with those from others suggest that there may be multiple pathways of ATZ storage and degradation. In conclusion, we have defined the IB as a major ATZ retention organelle that is different from the main ER and from classical autophagosomes and lysosomes. Understanding the molecular composition of the IB and further investigating the mechanisms of IB formation is likely to progress our knowledge on the mechanism by which serpin aggregates induce cell toxicity.

ACKNOWLEDGMENTS

We are grateful to Dr. Jennifer Lippincott-Schwartz (National Institute of Child Health and Human Development, National Institutes of Health, Bethesda, MD) for the kind gift of the plasmid LAMP-1-GFP; to Dr. Tamotsu Yoshimori (Department of Cell Genetics, National Institute of Genetics, Mishima, Japan) for the kind gift of the plasmid LC3-GFP; to Dr. Raquel Granell (Department of Social Medicine, University of Bristol, Bristol, United Kingdom) for help with statistics and analysis of data; and to Jim Paladino (BioVision Technologies, Exton, PA) for help with IPLab software. This work was supported by National Institutes of Health grant R01-DK-53293, by the Arkansas Tobacco Settlement (to G.B.), and by a postdoctoral grant from the Secretaria de Estado de Universidades Del Ministerio de Educacion y Ciencia, Spain (to S.G.).

REFERENCES

Arrasate, M., Mitra, S., Schweitzer, E. S., Segal, M. R., and Finkbeiner, S. (2004). Inclusion body formation reduces levels of mutant huntingtin and the risk of neuronal death. Nature *431*, 805–810.

Baldini, G., Martelli, A. M., Tabellini, G., Horn, C., Machaca, K., Narducci, P., and Baldini, G. (2005). Rabphilin localizes with the cell actin cytoskeleton and stimulates association of granules with F-actin cross-linked by α-actinin. J. Biol. Chem. *280*, 34974–34984.

Baldini, G., Wang, G., Weber, M., Zweyer, M., Bareggi, R., Witkin, J. W., and Martelli, A. M. (1998). Expression of Rab3D N135I inhibits regulated secretion of ACTH in AtT-20 cells. J. Cell Biol. *140*, 305–313.

Bennett, E. J., Bence, N. F., Jayakumar, R., and Kopito, R. R. (2005). Global impairment of the ubiquitin-proteasome system by nuclear or cytoplasmic protein aggregates precedes inclusion body formation. Mol Cell *17*, 351–365.

Cabral, C. M., Choudhury, P., Liu, Y., and Sifers, R. N. (2000). Processing by endoplasmic reticulum mannosidases partitions a secretion-impaired glycoprotein into distinct disposal pathways. J. Biol. Chem. *275*, 25015–25022.

Cabral, C. M., Liu, Y., Moremen, K. W., and Sifers, R. N. (2002). Organizational diversity among distinct glycoprotein endoplasmic reticulum-associated degradation programs. Mol. Biol. Cell *13*, 2639–2650.

Carrell, R. W. (2005). Cell toxicity and conformational disease. Trends Cell Biol. *15*, 574–580.

Chevrier, D., Fournier, H., Nault, C., Zollinger, M., Crine, P., and Boileau, G. (1991). Expression of porcine pro-opiomelanocortin in mouse neuroblastoma (Neuro2A) cells: targeting of the foreign neuropeptide to dense-core vesicles. Mol. Cell. Endocrinol. *79*, 109–118.

Davis, R. L. *et al*. (1999). Familial dementia caused by polymerization of mutant neuroserpin. Nature *401*, 376–379.

Diaz-Hernandez, M., Valera, A. G., Moran, M. A., Gomez-Ramos, P., Alvarez-Castelao, B., Castano, J. G., Hernandez, F., and Lucas, J. J. (2006). Inhibition of 26S proteasome activity by huntingtin filaments but not inclusion bodies isolated from mouse and human brain. J. Neurochem. *98*, 1585–1596.

Dickson, K. M., Bergeron, J. J., Shames, I., Colby, J., Nguyen, D. T., Chevet, E., Thomas, D. Y., and Snipes, G. J. (2002). Association of calnexin with mutant peripheral myelin protein-22 ex vivo: a basis for "gain-of-function" ER diseases. Proc. Natl. Acad. Sci. USA *99*, 9852–9857.

Feldmann, G., Bignon, J., Chahinian, P., Degott, C., and Benhamou, J. P. (1974). Hepatocyte ultrastructural changes in alpha1-antitrypsin deficiency. Gastroenterology *67*, 1214–1224.

Futerman, A. H., and Banker, G. A. (1996). The economics of neurite outgrowth–the addition of new membrane to growing axons. Trends Neurosci. *19*, 144–149.

Hidvegi, T., Schmidt, B. Z., Hale, P., and Perlmutter, D. H. (2005). Accumulation of mutant alpha1-antitrypsin Z in the endoplasmic reticulum activates caspases-4 and -12, NFkappaB, and BAP31 but not the unfolded protein response. J. Biol. Chem. *280*, 39002–39015.

Hosokawa, N., Wada, I., Natsuka, Y., and Nagata, K. (2006). EDEM accelerates ERAD by preventing aberrant dimer formation of misfolded alpha1-antitrypsin. Genes Cells *11*, 465–476.

Hultcrantz, R., and Mengarelli, S. (1984). Ultrastructural liver pathology in patients with minimal liver disease and alpha 1-antitrypsin deficiency: a comparison between heterozygous and homozygous patients. Hepatology *4*, 937–945.

Huntington, J. A., Pannu, N. S., Hazes, B., Read, R. J., Lomas, D. A., and Carrell, R. W. (1999). A 2.6 A structure of a serpin polymer and implications for conformational disease. J. Mol. Biol. *293*, 449–455.

Kabeya, Y., Mizushima, N., Ueno, T., Yamamoto, A., Kirisako, T., Noda, T., Kominami, E., Ohsumi, Y., and Yoshimori, T. (2000). LC3, a mammalian

homologue of yeast Apg8p, is localized in autophagosome membranes after processing. EMBO J. *19*, 5720–5728.

Kamimoto, T., Shoji, S., Hidvegi, T., Mizushima, N., Umebayashi, K., Perlmutter, D. H., and Yoshimori, T. (2006). Intracellular inclusions containing mutant alpha1-antitrypsin Z are propagated in the absence of autophagic activity. J. Biol. Chem. *281*, 4467–4476.

Kopito, R. R., and Ron, D. (2000). Conformational disease. Nat. Cell Biol. *2*, E207–E209.

Kopito, R. R., and Sitia, R. (2000). Aggresomes and Russell bodies. Symptoms of cellular indigestion? EMBO Rep. *1*, 225–231.

Kozutsumi, Y., Segal, M., Normington, K., Gething, M. J., and Sambrook, J. (1988). The presence of malfolded proteins in the endoplasmic reticulum signals the induction of glucose-regulated proteins. Nature *332*, 462–464.

Lee, A. S. (2005). The ER chaperone and signaling regulator GRP78/BiP as a monitor of endoplasmic reticulum stress. Methods *35*, 373–381.

Lee, C., Ferguson, M., and Chen, L. B. (1989). Construction of the endoplasmic reticulum. J. Cell Biol. *109*, 2045–2055.

Liu, Y., Choudhury, P., Cabral, C. M., and Sifers, R. N. (1997). Intracellular disposal of incompletely folded human alpha1-antitrypsin involves release from calnexin and post-translational trimming of asparagine-linked oligosaccharides. J. Biol. Chem. *272*, 7946–7951.

Liu, Y., Choudhury, P., Cabral, C. M., and Sifers, R. N. (1999). Oligosaccharide modification in the early secretory pathway directs the selection of a misfolded glycoprotein for degradation by the proteasome. J. Biol. Chem. *274*, 5861–5867.

Lomas, D. A. (2005). Molecular mousetraps, alpha1-antitrypsin deficiency and the serpinopathies. Clin Med. *5*, 249–257.

Lomas, D. A., Belorgey, D., Mallya, M., Miranda, E., Kinghorn, K. J., Sharp, L. K., Phillips, R. L., Page, R., Robertson, A. S., and Crowther, D. C. (2005). Molecular mousetraps and the serpinopathies. Biochem. Soc. Trans. *33*, 321–330.

Lomas, D. A., Evans, D. L., Finch, J. T., and Carrell, R. W. (1992). The mechanism of Z alpha 1-antitrypsin accumulation in the liver. Nature *357*, 605–607.

Manders, E. M., Stap, J., Brakenhoff, G. J., van Driel, R., and Aten, J. A. (1992). Dynamics of three-dimensional replication patterns during the S-phase, analysed by double labelling of DNA and confocal microscopy. J. Cell Sci. *103*, 857–862.

Martelli, A. M., Baldini, G., Tabellini, G., Koticha, D., Bareggi, R., and Baldini, G. (2000). Rab3A and Rab3D control the total granule number and the fraction of granules docked at the plasma membrane in PC12 cells. Traffic *1*, 976–986.

Mattioli, L., Anelli, T., Fagioli, C., Tacchetti, C., Sitia, R., and Valetti, C. (2006). ER storage diseases: a role for ERGIC-53 in controlling the formation and shape of Russell bodies. J. Cell Sci. *119*, 2532–2541.

Meusser, B., Hirsch, C., Jarosch, E., and Sommer, T. (2005). ERAD: the long road to destruction. Nat. Cell Biol. *7*, 766–772.

Miranda, E., Romisch, K., and Lomas, D. A. (2004). Mutants of neuroserpin that cause dementia accumulate as polymers within the endoplasmic reticulum. J. Biol. Chem. *279*, 28283–28291.

Mizushima, N., Yamamoto, A., Matsui, M., Yoshimori, T., and Ohsumi, Y. (2004). In vivo analysis of autophagy in response to nutrient starvation using transgenic mice expressing a fluorescent autophagosome marker. Mol. Biol. Cell *15*, 1101–1111.

Mohammad, S., Baldini, G., Granell, S., Narducci, P., Martelli, A. M., and Baldini, G. (2007). Constitutive traffic of melanocortin-4 receptor in Neuro2A cells and immortalized hypothalamic neurons. J. Biol. Chem. *282*, 4963–4974.

Moore, H. P., Walker, M. D., Lee, F., and Kelly, R. B. (1983). Expressing a human proinsulin cDNA in a mouse ACTH-secreting cell. Intracellular storage, proteolytic processing, and secretion on stimulation. Cell *35*, 531–538.

Mori, K. (2003). Frame switch splicing and regulated intramembrane proteolysis: key words to understand the unfolded protein response. Traffic *4*, 519–528.

Oda, Y., Hosokawa, N., Wada, I., and Nagata, K. (2003). EDEM as an acceptor of terminally misfolded glycoproteins released from calnexin. Science *299*, 1394–1397.

Okada, T., Yoshida, H., Akazawa, R., Negishi, M., and Mori, K. (2002). Distinct roles of activating transcription factor 6 (ATF6) and double-stranded RNA-activated protein kinase-like endoplasmic reticulum kinase (PERK) in transcription during the mammalian unfolded protein response. Biochem. J. *366*, 585–594.

Papp, E., Szaraz, P., Korcsmaros, T., and Csermely, P. (2006). Changes of endoplasmic reticulum chaperone complexes, redox state, and impaired protein disulfide reductase activity in misfolding alpha1-antitrypsin transgenic mice. FASEB J. *20*, 1018–1020.

Patterson, G. H., and Lippincott-Schwartz, J. (2002). A photoactivatable GFP for selective photolabeling of proteins and cells. Science *297*, 1873–1877.

Pattingre, S., Tassa, A., Qu, X., Garuti, R., Liang, X. H., Mizushima, N., Packer, M., Schneider, M. D., and Levine, B. (2005). Bcl-2 antiapoptotic proteins inhibit Beclin 1-dependent autophagy. Cell *122*, 927–939.

Pelham, H. R. (1996). The dynamic organisation of the secretory pathway. Cell Struct. Funct. *21*, 413–419.

Perlmutter, D. H. (2002a). The cellular response to aggregated proteins associated with human disease. J. Clin Invest. *110*, 1219–1220.

Perlmutter, D. H. (2002b). Liver injury in alpha1-antitrypsin deficiency: an aggregated protein induces mitochondrial injury. J. Clin Invest. *110*, 1579–1583.

Reyes, F., Marchant, L., Norambuena, L., Nilo, R., Silva, H., and Orellana, A. (2006). AtUTr1, a UDP-glucose/UDP-galactose transporter from *Arabidopsis thaliana*, is located in the endoplasmic reticulum and up-regulated by the unfolded protein response. J. Biol. Chem. *281*, 9145–9151.

Ruddock, L. W., and Molinari, M. (2006). N-glycan processing in ER quality control. J. Cell Sci. *119*, 4373–4380.

Rudnick, D. A., and Perlmutter, D. H. (2005). Alpha-1-antitrypsin deficiency: a new paradigm for hepatocellular carcinoma in genetic liver disease. Hepatology *42*, 514–521.

Schmidt, B. Z., and Perlmutter, D. H. (2005). Grp78, Grp94, and Grp170 interact with alpha1-antitrypsin mutants that are retained in the endoplasmic reticulum. Am. J. Physiol. *289*, G444–G455.

Schroder, M., and Kaufman, R. J. (2005). The mammalian unfolded protein response. Annu. Rev. Biochem. *74*, 739–789.

Schweizer, A., Ericsson, M., Bachi, T., Griffiths, G., and Hauri, H. P. (1993). Characterization of a novel 63 kDa membrane protein. Implications for the organization of the ER-to-Golgi pathway. J. Cell Sci. *104*, 671–683.

Sifers, R. N. (2004). Insights into checkpoint capacity. Nat. Struct. Mol. Biol. *11*, 108–109.

Teckman, J. H., An, J. K., Blomenkamp, K., Schmidt, B., and Perlmutter, D. (2004). Mitochondrial autophagy and injury in the liver in alpha 1-antitrypsin deficiency. Am J. Physiol. *286*, G851–G862.

Teckman, J. H., Gilmore, R., and Perlmutter, D. H. (2000). Role of ubiquitin in proteasomal degradation of mutant alpha(1)-antitrypsin Z in the endoplasmic reticulum. Am. J. Physiol. *278*, G39–G48.

Teckman, J. H., and Perlmutter, D. H. (2000). Retention of mutant alpha(1)-antitrypsin Z in endoplasmic reticulum is associated with an autophagic response. Am J. Physiol. *279*, G961–G974.

Wang, G., Witkin, J. W., Hao, G., Bankaitis, V. A., Scherer, P. E., and Baldini, G. (1997). Syndet is a novel SNAP-25 related protein expressed in many tissues. J. Cell Sci. *110*, 505–513.

Yorimitsu, T., and Klionsky, D. J. (2005). Autophagy: molecular machinery for self-eating. Cell Death Differ. 12 (Suppl 2), 1542–1552.

Yunis, E. J., Agostini, R. M., Jr., and Glew, R. H. (1976). Fine structural observations of the liver in alpha-1-antitrypsin deficiency. Am. J. Pathol. *82*, 265–286.

Zuber, C., Cormier, J. H., Guhl, B., Santimaria, R., Hebert, D. N., and Roth, J. (2007). EDEM1 reveals a quality control vesicular transport pathway out of the endoplasmic reticulum not involving the COPII exit sites. Proc. Natl. Acad. Sci. USA *104*, 4407–4412.

Zuber, C., Fan, J. Y., Guhl, B., and Roth, J. (2004). Misfolded proinsulin accumulates in expanded pre-Golgi intermediates and endoplasmic reticulum subdomains in pancreatic beta cells of Akita mice. FASEB J. *18*, 917–919.